The Proceedings of the International Conference on Creationism

Volume 8
Print Reference: Pages 707-730

Article 14

2018

Numerical Investigation of Strength-reducing Mechanisms of Mantle Rock During the Genesis Flood

Noah Cho
Center for Advanced Vehicular Systems, Mississippi State University

John Baumgardner
Logos Research Associates

Jesse Sherburn
U.S. Army Engineer Research and Development Center

Mark Horstemeyer
Department of Mechanical Engineering, Mississippi State University

Cho, N., J. Baumgardner, J.A. Sherburn, and M.F. Horstemeyer. 2018. Numerical investigation of strength-reducing mechanisms of mantle rock during the Genesis Flood. In *Proceedings of the Eighth International Conference on Creationism*, ed. J.H. Whitmore, pp. 707–730. Pittsburgh, Pennsylvania: Creation Science Fellowship.

NUMERICAL INVESTIGATION OF STRENGTH-REDUCING MECHANISMS OF MANTLE ROCK DURING THE GENESIS FLOOD

Noah Cho, 61 Nicklaus Ln., Starkville, MS 39759, USA HeechenECho@gmail.com
John Baumgardner, 24515 Novato Place, Ramona, CA 92065, USA
Jesse A. Sherburn, 3909 Halls Ferry Rd, Vicksburg, MS 39180, USA
Mark F. Horstemeyer, 1292 Chapel Hill Rd, Starkville, MS 39759, USA

ABSTRACT

This paper reports our efforts to model the effects of grain size, recrystallization, creep, and texture on overall rock strength within the Earth's mantle during the Genesis Flood. Our study uses experimental rheological data obtained from the mineralogical literature for olivine, which is an important mantle mineral. We apply an Internal State Variable (ISV) constitutive model within the framework of the TERRA finite element code to capture the subscale structures and their associated dynamics, strength, and viscosity effects during the Flood episode. Our numerical investigations, in both 2D and 3D, that include the improved deformation model reveal even more clearly that the potential for mantle instability enabled an episode of catastrophic plate tectonics to occur. This mantle instability arises from the extreme weakening behavior resulting from the relationship between microstructural features (herein texture, recrystallization, and grain size) and thermomechanical properties (e.g., stress and viscosity) under the conditions of temperature, pressure, and strain rate within the mantle during the Genesis Flood. It is our conviction that such an episode played a major role in the global Flood described in Genesis 7-8.

KEY WORDS

mantle rheology, Internal State Variable model, catastrophic plate tectonics, Genesis Flood, TERRA earth model

INTRODUCTION

The deformational behavior of rock under stress, that is, its rheology, plays a central role in the internal dynamics of the earth. Rock deformation is determined by the thermomechanical properties (e.g., elasticity, plasticity, viscosity, creep, and damage) of the minerals comprising the rock. Thermomechanical properties, in turn, are influenced profoundly by microstructural features such as grain size, phase transformations, dislocations, and texture (crystallographic orientation). Interestingly, many of these microstructural features can result in orders-of-magnitude reductions in rock strength, such that the mantle as a whole deforms in a catastrophic manner (Baumgardner 1994). Because mantle rocks are polycrystalline and microstructural properties of individual constituent minerals play important roles, a comprehensive deformation model (Horstemeyer 1998) capable of handling all these microstructural variations is needed to explore the weakening mechanisms with scientific rigor (Horstemeyer et al. 2002). A central focus of this paper is a description of such a comprehensive deformation model that may be applied to the runaway dynamics and catastrophic plate tectonics of the Genesis Flood.

The concept of Catastrophic Plate Tectonics (CPT) was introduced in Baumgardner (1986) and has been developed and refined over the past three decades (Austin et al. 1994). Numerical simulations, both in 2D and 3D, have provided deeper insights into the weakening mechanisms that physically allow a runaway process to occur (Baumgardner 2003). However, previous simulations have employed simple deformation models based on thermally activated diffusional and strain-rate creep and a constant yield stress that assume no interactions among mineral phases. Sherburn et al. (2011) showed that the creep models widely used in the geophysics community typically do not capture elasticity, work hardening, and damage (e.g., faulting), even though these deformation mechanisms play significant roles. However, today more realistic models exist, especially within the metallurgical and engineering communities that do include these phenomena. Sherburn et al. (2011) presented a new constitutive model for the earth's mantle, called an Internal State Variable (ISV) constitutive model that includes elasticity, plasticity, and creep regimes. Later, Sherburn et al. (2013) applied this ISV model to evaluate candidate weakening mechanisms related to static and dynamic recovery of dislocations in the mineral olivine. Despite that progress, many important features such as multiple mineral phases, variable grain size, and elastic stress limit (yield surface) models with pressure and temperature dependence had not yet been studied.

This paper reports results of investigations that apply the ISV model with structure-property relations calibrated against experimental mineral data from the literature for olivine, which is the most important upper-mantle mineral in the framework of the TERRA finite element code. We explore the effects of grain size, creep, and texture (arising from plastic spin) on overall rock strength under possible conditions that existed in the mantle during the Genesis Flood. This study provides crucial new understanding on how the subscale heterogeneous structures and thermomechanical properties cooperatively act together to produce the extreme weakening that allowed the global Flood cataclysm to unfold as it did.

MATERIALS AND METHODS

1. Dependence of mechanical properties on microstructure

The mechanical properties of solids such as strength and viscosity are significantly influenced by their hierarchical multiscale structures,

their morphology, and their stereology. When a solid (such as rock or metal) is subjected to stress, it first deforms elastically up to a certain point and then it deforms inelastically. Because the deformations that occur in the mantle typically are huge relative to the elastic limit (i.e., boundary between elasticity and inelasticity), we will be concerned primarily with inelastic deformation. In this study, we focus on the plastic deformation among the inelastic mechanisms. The plastic responses of mantle rocks depend in a fundamental way on several subscale heterogeneous structures and their interactions that can be coupled together on different spatial scales. In this section, some important multiscale features and their associated mechanisms that occur during plastic deformation, especially in the earth's mantle, are briefly explained in order of length scale, from smallest to largest.

A. Dislocations

When polycrystalline materials like rocks deform plastically under stress, line defects at the atomic scale are generated within grains and at grain boundaries. These defects are known as "dislocations," because the crystalline lattice is dislocated along a 1D line of atoms. Under certain thermomechanical conditions, these dislocations move in the grains to stabilize the material's thermodynamic free energy and their motions lead to a reduction in the rock's strength. The microstructural mechanisms related to these motions are referred to as "recovery." Generally speaking, the number density of dislocations increases under deformation, and the interactions among dislocations as they move highly affect the material's strength. In most cases, dislocation interaction increases the material's strength, and this phenomenon is known as "work hardening." During plastic deformation the material simultaneously undergoes both hardening due to dislocation interactions and weakening due to the recovery and annihilations of dislocations. The material's strength is therefore determined by a competition between the two processes of hardening and recovery. Hence, understanding dislocation mobility, their density changes, and their interactions are crucial to correctly representing a material's mechanical properties.

B. Grains

Polycrystalline rocks have stable crystal structures, and each individual crystal is known as a "grain." Each grain in a rock has a specific shape, size, and orientation and shares polygonal boundaries with its neighboring grains. Grain boundaries can act as either a source or sink for dislocations. The diameter of a grain, called its grain size, affects the work hardening rate, because the boundaries act as barriers to inhibit dislocation motion. Hence, as the grain size decreases, the work hardening rate increases because the dislocations have less room to move (Hall 1951, 1954; Petch 1953). This Hall-Petch effect can be succinctly stated that as the grain size increases, the material weakens.

Under certain thermomechanical conditions (e.g., pressure, temperature, and dislocation density), the grain boundaries can migrate to find energetically stable states. That is, the grain size changes until it finds a saturated state. This phenomenon is known as "grain boundary migration" or "grain growth." Generally, under high temperature, the grain size increases as larger grains consume adjacent smaller grains. Under high pressure, grain growth is inhibited, however, because the thermodynamic activation energy barrier for the grain growth is raised. Hence, the resultant grain growth depends upon multiple thermomechanical quantities.

In addition to grain growth, grain size reduction (or refinement) can also take place as a consequence of plastic deformation. This occurs when new small grains nucleate inside of the original grains or at the grain boundary. This phenomenon is known as "dynamic recrystallization." For a geological example, dynamically recrystallized microstructures with very fine grains are commonly observed in highly deformed rocks like mylonite, a metamorphic rock found in zones of high shear such as folds or faults. Many laboratory studies have shown that dynamic recrystallization indeed occurs with dramatic grain size reduction (Hansen et al. 2012; Karato et al. 1980; Ohuchi et al. 2015; Van der Wal et al. 1993; Zhang et al. 2000).

C. Crystallographic Preferred Orientation (CPO) or texture

As discussed earlier, each grain of a polycrystalline material has its own orientation. However, during plastic deformation, the grains undergo rotations so that the grains display a distinctive average orientation. This distribution of grain orientations is known as "deformation-induced crystallographic preferred orientation (CPO)" (Karato 2012). In geophysical studies, researchers compare CPO observed in laboratory studies with the seismological wave data from the mantle to gain insight into the mantle's plastic deformation history (Mainprice et al. 2000). A high-fidelity model able to predict the CPOs of mantle minerals for various types of deformation could potentially utilize seismic observations from today's mantle to gain important insight into the mantle's deformation that occurred during the Flood cataclysm.

D. Mineralogical compositions of the earth's mantle

The earth's mantle is thought to comprise at least eleven different minerals across its depth (Karato 2012; Ringwood 1991; Stixrude and Lithgow-Bertelloni 2011). As the depth increases, the dominant upper mantle minerals (olivine, pyroxenes, and garnet) undergo phase changes to other minerals with different crystalline structures due to increased pressure and temperature. These physical changes are known as "solid-solid phase transformations."

Most of these phase changes occur in the lower portion of the upper mantle between depths of 410 and 660 km, a region known as the mantle transition zone. The three main transition zone minerals are wadsleyite, ringwoodite, and majorite (Al-deficient garnet). Small amounts of clinopyroxene and Ca-perovskite can appear in the upper and lower portions of the transition zone, respectively (Irifune et al. 2008; Wood and Helffrich 2001). Since the dominant mineral phase in the upper mantle is olivine (approximately 60% in volume fraction), its various phases play significant roles throughout the mantle. At 410 km depth, where the transition zone begins, olivine first transforms to wadsleyite. Near 520 km depth, wadsleyite further transforms to ringwoodite, which has a spinel structure. Near 660 km depth, ringwoodite decomposes into Mg-perovskite and ferropericlase. This phase transition marks the boundary between the transition zone and the lower mantle. Also in the 600-700 km depth interval, Ca-perovskite exsolves from the majoritic garnet, and some portion of the garnet transforms to Mg-perovskite. Consequently, the lower mantle consists approximately of 70% Mg-perovskite, 20% ferropericlase, and 10% Ca-

perovskite. The overall mineralogical volume fraction map of the earth's mantle is shown in Fig. 1.

With this mineralogical structure of the mantle in view, the inelastic mechanical responses of rocks obviously depend on the different length scales of structures embedded within each of its constituent minerals. As already mentioned, a rock's plastic response to stress depends on dislocation mobility and interaction, grain size and grain boundary-dislocation interactions, and crystallographic preferred orientations. These in turn depend on pressure, temperature, strain rate (deformation rate), stress state, and mineralogical composition. Representing these dependencies and processes in an accurate manner is key to realistic modeling of catastrophic mantle dynamics and the associated plate tectonics during the Genesis Flood. The following section addresses the relationships between crystalline microstructures and the primary mechanisms by which rocks deform.

2. Important deformational mechanisms

The complex manner in which minerals deform, combined with extreme pressures and temperatures of the earth's interior, together with the fact that mineral compositions vary with depth make modeling mantle dynamics in a realistic manner a daunting challenge. Compounding this challenge is the fact that mechanical properties of all the relevant minerals cannot be easily measured. With these challenges in mind this study focuses on several crucial rheological mechanisms that must have played key roles during the worldwide Flood cataclysm.

A. Plasticity and creep

In physics and materials science, plastic deformation refers to the irreversible changes of shape of a solid in response to applied forces. Elastic deformation, by contrast, refers to the changes in shape from applied forces that disappear entirely when the applied forces are removed. When plastic deformation occurs, dislocations nucleate and their interactions either hinder their mutual motions (hardening) or annihilate one another (recovery). When the dislocation density and their interactions increase, dislocation motion can be inhibited, such that a solid's resistance to further deformation increases. This increased resistance arising from interactions among dislocations increases the work hardening. Work hardening typically increases as the strain rate and pressure increase but decreases as the temperature increases. On the other hand, more recovery can occur when the strain rate decreases, the pressure decreases, and the temperature increases (Karato 2012; Kirby 1983). In the case of the earth's mantle, where there are persisting stresses and ongoing irreversible deformation of the rock material, both creation of new dislocations and annihilation of existing dislocations are continuously taking place.

In the earth's mantle, complicated thermal and mechanical states exist together. As the depth increases, the temperature and pressure simultaneously increase, and the competition between dislocation creation and annihilation determines the resulting rock strength at each depth. Because the strain rate during the Genesis Flood was dramatically greater than at present, the influences of strain rate on the strength of mantle rock at the time of the Flood are also of paramount importance.

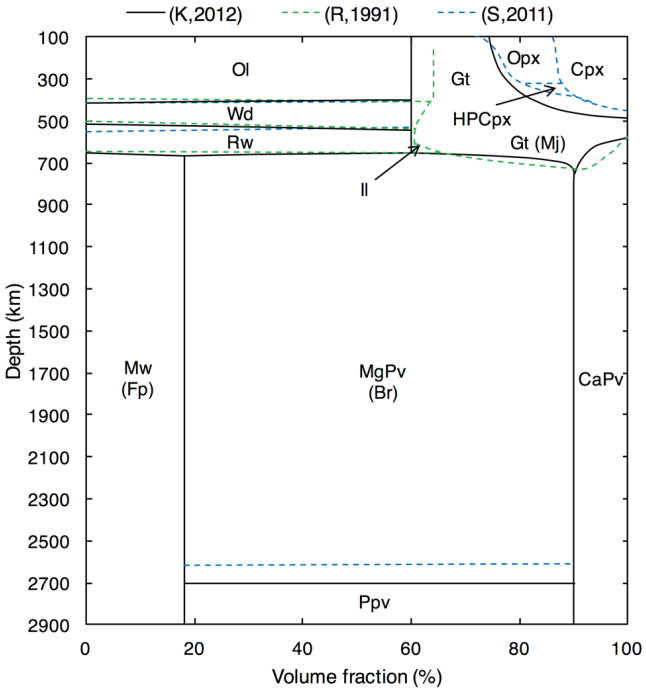

Figure 1. Constitutional map of important minerals in the Earth's mantle. The volume fraction of each mineral has been obtained by observations from geochemistry, geophysics, and experimental studies at the mantle like pressure and temperature conditions (Karato, 2012; Ringwood, 1991; Stixrude and Lithgow-Bertelloni, 2011). The most dominant minerals are olivine (Ol), wadsleyite (Wd), ringwoodite (Rw), Mg-perovskite (MgPv), and post-perovskite (Ppv) at their corresponding depths. The abbreviations for the data references represent that K,2012 for Karato (2012), R,1991 for Ringwood (1991), and S,2011 for Stixrude and Lithgow-Bertelloni (2011). Ol, olivine; Opx, orthopyroxene; Cpx, clinopyroxene; HPCpx, high pressure clinopyroxene; Gt, garnet; Mj, majorite; Wd, wadsleyite; Rw, ringwoodite; Mw, magnesiowüstite; Fp, ferropericlase; MgPv, magnesium perovskite; Br, bridgmanite; CaPv, calcium perovskite; Ppv, post-perovskite.

B. Recrystallization, dislocation-grain boundary interaction, and grain boundary sliding

As the temperature increases, new crystal grains are nucleated, and their sizes grow (recrystallization) consuming dislocations (i.e., plastically stored energy) and smaller grains. Because this recrystallization process decreases the dislocation density, the mantle's strength also decreases when recrystallization takes place. The process of recrystallization is affected by pressure, temperature, strain rate, and dislocation density. As the pressure increases, recrystallization is inhibited due to the increase in activation energy. By contrast, as the temperature and the dislocation density increase, the recrystallization rate increases. The strain rate effect is more complicated, but, in general, the static component of recrystallization increases as the strain rate decreases, while its dynamic component increases as the strain rate increases (Derby and Ashby 1987; Doherty et al. 1997).

As mentioned earlier, the interactions between dislocations and grain boundaries can harden the rock. As the grain size decreases, the total surface area of grain boundaries increases, so that the likelihood of dislocation-grain boundary interactions increases. This effect causes the dislocation density to increase and the rock strength also to increase. Since the grain size depends on temperature, pressure, strain rate, and dislocation density, the strength change associated with dislocation-grain boundary interactions kinetics is also a function of these factors. Conversely, because the diffusion rate of point defects increases when grain size is small, the strength of rock can also decrease when the grain size is small. Because the mineral crystal is covalently bonded, dislocation movement tends to be slow such that the diffusion of point defects can become more important than the interactions between grain boundaries and dislocations. Therefore, both these competing mechanisms (weakening and hardening at a certain size of grain) must to be taken into account.

During the Genesis Flood, the high strain rates most likely favored grain size reduction. Under conditions of high strain rate and moderate temperature that likely prevailed in the upper mantle, the dynamic recrystallization process would have resulted in grain size reduction. Once the grain size is small, other grain size sensitive mechanisms like "grain boundary sliding" can become dominant. Indeed, recent studies (Hansen et al. 2012; Ohuchi et al. 2015) on the deformation of mantle rocks suggest that grain boundary sliding may be one of the primary deformation mechanisms in the upper mantle.

C. Effects of texture (deformation-induced CPO)

Another mechanism that can greatly reduce rock strength in the mantle is the deformation-induced CPO. During plastic deformation, the grains rotate at different rates, so the rock ultimately has a distinctive average grain orientation within a distribution of orientations. As explained earlier, a rock's viscous strength is related to its resistance to further deformation. When the deformation-induced CPO is developed (i.e., when the grains are spinning plastically), resistance to deformation and hence the material strength is reduced. In the mechanics and material science community, these texture effects are also referred to as the "plastic spin" at the microscale (Dafalias 2000) and as "torsional softening" at the macroscale. The latter term has come into use because the stress-weakening effects are more prominent under torsional (shear) deformation than under uniaxial compressive or tensional deformation (Horstemeyer and McDowell 1998). This texture effect may have played an important role during the Flood, especially in regions of the mantle that experienced exceptional amounts of mechanical shear.

D. Phase transformation and multicompositional effects

When a phase transformation takes place, the newly nucleated minerals initially have a tiny average grain size with a very low dislocation density. The dominant deformation mechanisms such as grain boundary sliding and diffusion creep in these small grains significantly reduce the material's strength. This argues that notable strength weakening ought to occur at phase change boundaries. Moreover, experimental observations pertaining to grain growth kinetics (Hiraga et al. 2010; Ohuchi and Nakamura 2007; Tasaka and Hiraga 2013; Yamazaki et al. 2010) indicate that the grain growth rate is greatly reduced when a mineral is aggregated with other minerals. This suggests that, because most mantle rocks are composed of several different minerals, the actual grain growth rates in the mantle ought to be significantly smaller than what has been determined in the laboratory for single mineral compositions. Because such a large fraction of the mantle's volume passed through the transition zone during the Flood, one might expect that weakening from grain size reduction may have played a significant role not only during the Flood but also for several centuries afterward.

3. A constitutive model for rheology of the earth's mantle

As just discussed, multiple rheological mechanisms must have operated simultaneously in the mantle during the Flood. Because the interactions among mechanisms are so numerous and complex, a pencil and paper analysis is utterly incapable of yielding a confident level of understanding of the dynamics of the Flood cataclysm. Numerical simulations grounded in reliable observational data are necessary to explore such a complex problem. With this motivation, several authors (Baumgardner 2003; Sherburn et al. 2013) have developed numerical models in initial attempts to include some of the basic rheological mechanisms and explore the dynamics of earth's mantle and lithosphere during the Flood.

In particular, Sherburn et al. (2013) implemented a plasticity Internal State Variable (ISV) constitutive model originally developed at Sandia National Laboratories (Bammann 1990; Bammann et al. 1993; Horstemeyer 2000). This work demonstrated that the ISV model has an impressive capacity for capturing essential mechanical behavior of metals, polymers, and mantle rocks. The ISV model utilizes material history variables to track the elastic and the plastic attributes of a material, including its hardening and recovery mechanisms governed by the material's internal structure. From Sherburn et al. (2013), a crucial microstructural mechanism was identified that likely played a key role in the Genesis Flood event, namely, the dynamic recovery. The ISV model used in the study had been calibrated against experimentally measured stress-strain data for the upper mantle rock type known as lherzolite. With dynamic recovery turned on in the ISV model, the TERRA2D simulations showed dramatic strength weakening in the mantle and catastrophic overturn of the mantle within a time span of only a few weeks.

Our present study builds upon Sherburn et al. (2013) and includes additional rheological mechanisms that likely played important roles and also contributed to the rapid runaway process of the cataclysm. These additions include the following:

1) Pressure dependence on the yield strength (we model the yield strength using a yield surface concept that defines the boundary between elasticity and inelasticity in all directions), of the hardening, and of the recovery in the ISV equations. Also, the texture effect was included in the hardening to capture stress-state dependent mechanical behavior.

2) We added a recrystallization model to investigate its overall effects on the runaway process.

3) We added a grain size growth and reduction model that can track the grain size progression history. In this grain size model, the growth and reduction kinetics of olivine's grains are simultaneously calculated based on actual laboratory data, and the average grain size is determined from a competition between the grain size growth and reduction. The resulting average grain size in turn influences the rock strength.

What follows is a brief description of each of these additions to the overall ISV model.

A. Isotropic and kinematic hardening equations of the ISV constitutive model

A primary goal in the development of the ISV model was to capture the dislocation density changes that occur when a polycrystalline material is deformed. Toward that end, the ISV model attempts to represent as realistically as possible two main mechanisms related to the dislocation density change that simultaneously operate during the deformation: 1) hardening due to the dislocation density increase, and 2) weakening due to the dislocation density decrease. Work hardening occurs when the dislocations build up, while recovery occurs when the dislocations glide and annihilate on a slip plane (dynamic recovery) or climb on a slip plane that is perpendicular to the plane (static recovery). These two microstructural recovery mechanisms are essentially equivalent to the processes known within the geophysics community as dislocation creep and diffusion creep, respectively.

In the ISV model, two crucial quantities are the isotropic (κ) and kinematic (α̃) hardening, which represent stress-like quantities arising from accumulations of statistically stored (isotropic) dislocations and geometrically necessary (anisotropic) dislocations during the deformation, respectively. Two hardening rate equations in the ISV model each include a hardening and two recovery terms as follows:

$$\dot{\kappa} = \left[H(1-X)\left|\dot{\varepsilon}^{in}\right| - \left(\sqrt{2/3}\, R_d \left|\dot{\varepsilon}^{in}\right| + R_s\right)\kappa^2\right]\left(\frac{d_0}{d}\right)^z \quad (1)$$

$$\dot{\tilde{\alpha}} = \left[h(1-X)\dot{\varepsilon}^{in} - \left(\sqrt{2/3}\, r_d \left|\dot{\varepsilon}^{in}\right| + r_s\right)\tilde{\alpha}\left|\tilde{\alpha}\right|\right]\left(\frac{d_0}{d}\right)^z \quad (2)$$

where H is the isotropic work hardening, h is the kinematic work hardening, R_d is the isotropic dynamic recovery, r_d is the kinematic dynamic recovery, R_s is the isotropic static recovery, r_s is the kinematic static recovery, $\dot{\varepsilon}^{in}$ is the deviatoric inelastic strain rate, X is the recrystallized volume fraction, d_0 is the initial grain size, d is the current grain size, and z is the grain size-stress exponent. All the hardening and recovery terms are dependent on temperature and pressure. When the pressure increases, the total hardening rate increases; whereas when the temperature increases, the hardening rate decreases. As shown in both Eqs. (1) and (2), the recrystallization and the grain size effects are included. These equations show that increasing the volume fraction of recrystallized grains decreases the work hardening rate. Also, as the grain size increases, both work hardening and static recovery decrease by the same factor; therefore, competition between the two grain size effects are automatically incorporated. In summary, a reduction in hardening translates to a reduction in rock strength.

B. Recrystallization

Experimental studies on recrystallization, for both metals and rocks, find that the rate of recrystallized grain volume fraction change tends to obey the following relationship:

$$\dot{X} \propto X(1-X), \quad (3)$$

where X is the recrystallized grain volume fraction (Brown and Bammann 2012). When old grains recrystallize, previous dislocations are destroyed as new grains are formed. As mentioned in the preceding section, as the recrystallized volume fraction increases, the material strength decreases. Based on these ideas, we developed the following mathematical description of the recrystallization process:

$$\dot{X} = \dot{X}_{drx} + \dot{X}_{srx}, \quad (4)$$

$$\dot{X}_{drx} = c_{x1}\, exp\left(-\frac{c_{x2} + Pc_{dp}}{T}\right)[(\kappa^2 + |\tilde{\alpha}|^2)/\mu\,(P,T)]X^{c_{xa}}(X_\infty - X)^{c_{xb}}\left|\dot{\varepsilon}^{in}\right|, \quad (5)$$

$$\dot{X}_{srx} = c_{x3}\, exp\left(-\frac{c_{x4} + Pc_{sp}}{T}\right)[(\kappa^2 + |\tilde{\alpha}|^2)/\mu\,(P,T)]X^{c_{xa}}(X_\infty - X)^{c_{xb}}, \quad (6)$$

$$X_\infty = c_{x5}\, exp\left(-\frac{c_{x6}}{T}\right), \quad (7)$$

where $\dot{X}_{drx}$ is the dynamically recrystallized volume fraction progression rate, $\dot{X}_{srx}$ is the statically recrystallized volume fraction progression rate, μ is the shear modulus, X_∞ is the maximum volume fraction of recrystallization, c_{x1} and c_{x3} are the recrystallization rate constants of dynamic and static recrystallization, respectively, c_{x2} and c_{x4} are the temperature dependent constants, c_{dp} and c_{sp} are the pressure dependent constants, c_{xa} and c_{xb} are the sigmoidal shape constants, and c_{x5} and c_{x6} are the maximum recrystallized volume constants.

C. Grain size kinetics

Grain size kinetics can be divided into separate growth and reduction components. The model for grain growth kinetics is well established. Since this grain growth mechanism is driven by the thermodynamic energy, the following Arrhenius type equation is typically used:

$$\dot{d}_{grw} = \frac{1}{nd^{n-1}} k_0\, exp\left(-\frac{E_g^* + PV_g^*}{RT} + a(v_f)^b\right), \quad (8)$$

where d is the grain size, n is the grain growth exponent, k_0 is the grain growth rate constant, E_g^* is the activation energy for the grain growth, P is the pressure, V_g^* is the activation volume for the grain growth, R is the gas constant, T is the temperature, a and b are the constants of volume fraction effect in a multi-mineral composition

system, and v_f is the volume fraction of primary mineral (olivine in this study). Clearly, the rate of grain growth increases as the temperature increases, pressure decreases, and the volume fraction of the primary mineral increases.

Grain size reduction is logically related to dynamic recrystallization since dynamic recrystallization results in grain refinement. Therefore, we created a new formulation for the grain size reduction rate as follows:

$$\dot{d}_{red} = -X_{drx} c_{x9} d(\omega - d)^2 \left|\dot{\varepsilon}^{in}\right|, \tag{9}$$

$$\omega = c_{x7}\left[\left|\dot{\varepsilon}^{in}\right| exp\left(\frac{E_g^* + PV_g^*}{RT}\right)\right]^{-c_{x8}} \tag{10}$$

where X_{drx} is the dynamically recrystallized volume fraction, c_x is the reduction rate constant, and ω is the steady-state grain size. Therefore, the total average grain size rate of change is the sum of the grain growth rate $\dot{d}_{grw}$ and the grain size reduction rate $\dot{d}_{red}$

$$\dot{d} = \dot{d}_{grw} + \dot{d}_{red}. \tag{11}$$

The average grain size is used in the two hardening equations, Eqs. (1) and (2), as the model is stepped in time.

D. Grain size-stress relation

With changes in grain size during deformation, the degree of dislocation-grain boundary interactions and the diffusion rate also change. These mechanisms affect the rock strength. The relationship between the grain size and stress can be expressed as

$$\sigma = \sigma_0 \left(\frac{d_0}{d}\right)^z, \tag{12}$$

where σ_0 is the reference stress, d_0 is the reference grain size, and z is the exponent. In order to describe the grain size effect on the stress, Eq. (12) has been incorporated into the two hardening equations, Eqs. (1) and (2).

E. Texture effect and stress-state dependence

Anisotropy can develop during deformation and plays a significant role in reducing the rock's strength. The effect of anisotropy (i.e., plastic spin or torsional softening) therefore needs to be included in a mathematical description of mantle deformation. To treat this phenomenon, we employ the invariants of the deviatoric stress tensor in the same manner as Horstemeyer et al. (2000) used in their damage model. The second and third invariants of the deviatoric stress tensor are expressed

$$J_2 = \frac{1}{2} s_{ij} s_{ij} \tag{13}$$

and

$$J_3 = \frac{1}{3} s_{ij} s_{jk} s_{ki}, \tag{14}$$

where J_2 and J_3 are the second and third invariants, respectively, of the deviatoric stress tensor $\tilde{S}$, and the subscripts obey Einstein tensor notation. The hardening and dynamic recovery terms in the ISV isotropic and kinematic hardening equations are influenced by these two deviatoric stress invariants as follows:

$$h(P,T) = C_9\left[1 + C_a\left(\frac{4}{27} - \frac{J_3^2}{J_2^3}\right) + C_b \frac{J_3}{J_2^{1.5}}\right]\mu(T,P), \tag{15}$$

$$r_d(P,T) = C_7\left[1 - C_a\left(\frac{4}{27} - \frac{J_3^2}{J_2^3}\right) - C_b \frac{J_3}{J_2^{1.5}}\right] exp\left[-\frac{C_8 + PC_{21}}{T}\right], \tag{16}$$

$$H(P,T) = C_{15}\left[1 + C_a\left(\frac{4}{27} - \frac{J_3^2}{J_2^3}\right) + C_b \frac{J_3}{J_2^{1.5}}\right]\mu(T,P), \tag{17}$$

$$R_d(P,T) = C_{13}\left[1 - C_a\left(\frac{4}{27} - \frac{J_3^2}{J_2^3}\right) - C_b \frac{J_3}{J_2^{1.5}}\right] exp\left[-\frac{C_{14} + PC_{24}}{T}\right], \tag{18}$$

where h is the pressure and temperature dependent kinematic hardening term, C_9 is the material specific hardening rate constant, C_a is the torsional constant that differentiates torsional stress from other stress states, C_b is the tension/compression constant that differentiates tension and compression behavior, μ is the pressure and temperature dependent shear modulus, r_d is the dynamic recovery in the kinematic hardening, C_7 is the material-specific recovery rate constant, C_8 is the temperature sensitivity constant of the dynamic recovery, C_{21} is the pressure sensitive constant of the dynamic recovery, P is the hydrostatic pressure, T is the absolute temperature, H is the isotropic hardening term, C_{15} is the material-specific isotropic hardening rate constant, R_d is the dynamic recovery in the isotropic hardening, C_{13} is the material specific dynamic recovery rate constant, C_{14} is the temperature sensitivity constant, and C_{24} is the pressure sensitivity constant. Note that hardening terms h and H and recovery terms r_d and R_d appear in the hardening rate equations, Eqs. (1) and (2).

F. Model calibrations based on the experimental rheological data for olivine

The procedure by which one obtains the material specific parameters and constants required by a mathematical model to describe a physical process is known as model "calibration." For a calibration of the grain growth of olivine (or forsterite), we used the experimental data from Hiraga et al. (2010) and Tasaka and Hiraga (2013). Since their experiments were performed at temperatures comparable to those in the upper mantle, it is appropriate to use their data to calibrate the model temperature dependence. However, since the applied pressures in their experiments were very low compared to actual mantle pressures, their experimental results are not appropriate to calibrate the pressure dependence of grain growth kinetics. Hence, the pressure dependent parameter for the grain growth (i.e., activation volume) was simply set to a reasonable value, 3.0 x 10^{-6}, which is close to an average among the other mantle minerals: 3.8 x 10^{-6} for garnets (Yamazaki et al. 2010; Paladino and Maguire 1970), 0.2 x 10^{-6} for perovskites (Yamazaki et al. 1996; Wang et al. 1999), and 4.4 x10^{-6} for ferropericlase (Tsujino and Nishihara 2009; 2010). The calibrated model and the experimental data are shown in Fig. 2.

Next, the grain size effect on the rock's strength also requires calibration. Based on laboratory data for olivine (Hansen et al. 2012; Karato et al. 1980; Van der Wal et al. 1993), the relationship between the grain size and the strength of olivine could be analyzed by using Eq. (12). The best calibrated exponent z from these experimental data was 0.8. The comparison between the experimental data and the model is shown in Fig. 3.

With these calibrated constants and parameters, the stress-strain behavior at various temperatures, pressures, and strain rates was finally calibrated by using the ISV constitutive equations. Using

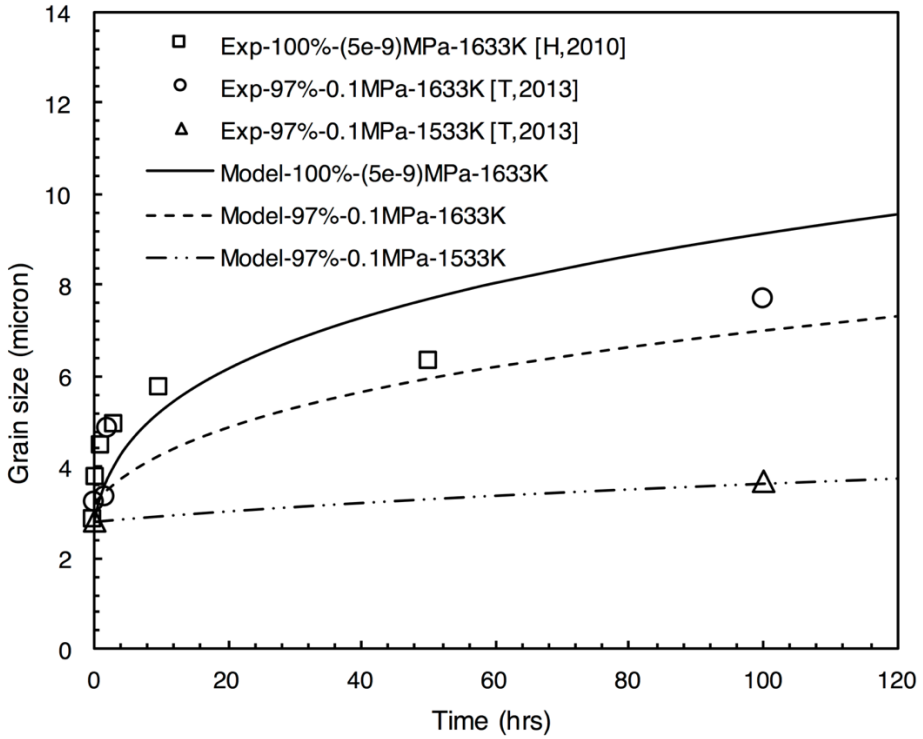

Figure 2. Static grain growth experimental data performed by Hiraga *et al.* (2010) and Tasaka & Hiraga (2013). Squares, circles, and triangles represent the experimental data at various temperatures and pressures. The lines show the calibrated model using Eq. (8) using the least-square method. Note that these data cannot provide a pertinent pressure dependence of olivine's static grain growth just because of the small range of pressures. Alternatively, we simply used an average dependence among the other mantle minerals for the pressure dependence (*i.e.*, activation volume of the grain growth process).

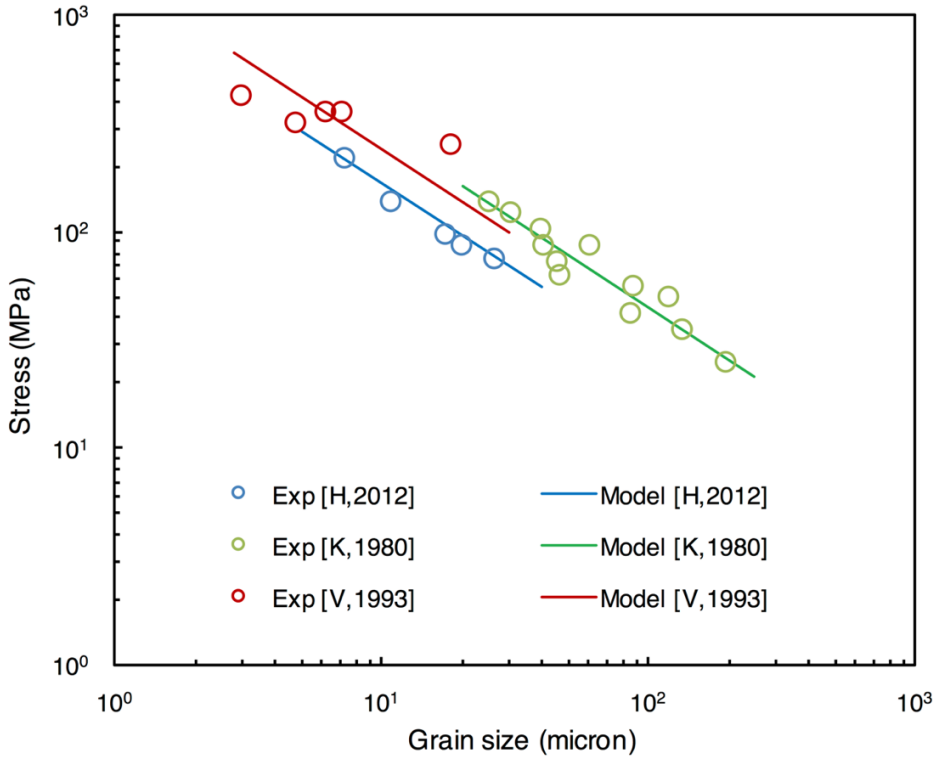

Figure 3. Relationship between the grain size and the stress of olivine on a log-log scale. As the grain size increases, the stress decreases. The deformation experiments were performed by Hansen *et al.* (2012), Karato *et al.* (1980), and Van der Wal *et al.* (1993) at different experimental conditions. These data yield a consistent value for the exponent z in Eq. (12) of 0.8, regardless of the experimental conditions.

experimental data from the literature for olivine, we were able to calibrate our ISV model including pressure sensitivity within the reported experimental uncertainty. Considering uncertainty is important, because of the lack of experimental recrystallization data at higher pressures. However, Hansen et al. (2012) demonstrated that the recrystallization process weakens more than 90% of total hardening in olivine aggregates under deformations at 1473 K in temperature and 300 MPa in pressure. Based on this observation, we chose pressure dependent parameters that cause the volume fraction of recrystallization gradually to decrease as the pressure increases. By this means the weakening from recrystallization in this model is made to agree with experimental measurements. The comparison between the experimental stress-strain behavior and our calibrated model is plotted in Fig. 4, and the constants and parameters are summarized in Table 1. Once the recrystallized volume fraction increases, the stress-strain behavior shows a concave downward shape (i.e., the slope decreases).

In the present study, olivine's properties alone were applied to the whole mantle, even though the mantle has multiple mineral constituents as well as important phase transitions. Hence, it is necessary for the present model to make large extrapolations of olivine's mineralogical and mechanical properties because the large ranges of pressure and temperature across the mantle. In order to alleviate the unrealistic predictions, some parameters for the hardening variables were slightly reduced to the strength level that the few experimental studies (e.g., Girard et al. 2016) provide for mantle-like temperature and pressure conditions.

G. Simulation setup in TERRA

Once the ISV model has been calibrated, the initial and boundary conditions for the finite element analysis using TERRA need to be identified. In particular, for the purposes of this work we sought to capture the mechanics instability and associated runaway behavior exhibited in the Flood cataclysm. In the TERRA2D simulations, we used a rectangular grid with approximately 131,000 elements (512 on the surface and 256 through the depth) corresponding to a domain 5,780 km in width and 2,890 km in depth as displayed in Fig. 6 (the element size was approximately 11 km). The TERRA3D calculations used a grid with approximately 1,400,000 cells with the shape of hexagonal prisms (33 spherical layers of cells in radial direction with 42,250 cells in each shell).

Regarding the initial microstructural states when the Flood started, more studies on these microstructural effects are frankly needed, because it is likely that microstructural rearrangements from flow and other processes in the mantle already had been taking place after the creation week until the Flood started. For example, the grains of the mantle rocks could have grown during that time from Day 3 of Creation until the Flood (~1600 years). Although these initial microstructural effects are not included in this paper, such effects might have played a crucial role in triggering the Flood itself (Horstemeyer et al. 2002). Regarding the initial grain size when the simulation started, it was simply set to 100 μm throughout the entire mantle. To alleviate numerical singularities, the statically and dynamically recrystallized volume fractions at the initial stage were set to a very low number, 5 x 10^{-7}, instead of zero. Also, the initial hardening variables were set to zero.

From a Biblical standpoint we have reason to suspect some uncertainty with the initial conditions in our simulations. The Bible seems to imply high rate, large, and complex deformation on Day 3 of Creation Week when God gathered the waters below the firmament together into one place and caused the dry land to appear. Such an event almost certainly would have generated major heterogeneities throughout the mantle. Because we have no way even of guessing what those variations in microstructural properties were like, in this paper, we therefore assume very simple and largely uniform initial conditions and focus on the mantle dynamics and related weakening effects that develop from that admittedly simplified initial state. In future simulations we will explore the different possible deformational histories prior to the Flood.

The viscosity in our numerical models depends on the local temperature, pressure, and strain rate. Assuming that the strain rate was very low before the Flood began, we prescribe a depth-dependent reference viscosity η using following equation:

$$\eta(P,T) = \eta_0 exp\left[-\frac{E_v^* + PV_v^*}{RT}\right], \quad (19)$$

where η_0 is the reference viscosity, E_v^* is the activation energy for the mantle's viscous response, P is the pressure, V_v^* is the activation volume for the pressure dependence, R is the gas constant, and T is the absolute temperature. In order to match closely the earth's current viscosity structure, separate values for E^* and V^* are applied to the upper mantle, mantle transition zone, and lower mantle (Baumgardner 1994). And the reference viscosity η_0 was set to 10^{23} Pa·s. The initial viscosity structure used in these simulations is shown in Fig. 5.

Also because we do not know what the temperature distribution within the earth might have been at the onset of the Flood, we assume an extremely simple initial temperature distribution as depicted in Fig. 6. This distribution corresponds to a horizontal variation in temperature across the computational domain of a single period of the cosine function as follows:

$$T(x,y) = T_{ref}(y) - 0.04\cos\left(\frac{\pi x}{w}\right) T_{ref}\left(\frac{h}{2}\right), \quad (20)$$

where T is the absolute temperature, x and y are the horizontal and vertical points of the mantle domain in the TERRA2D, respectively, T_{ref} is the depth dependent reference temperature profile to match the temperature gradient implied by the physical parameters from the Preliminary Reference earth Model (PREM) (Dziewonski and Anderson 1981), w and h are the width and height of the TERRA2D domain, respectively. We set the initial temperature to 300 K on the top surface and 3700 K at the core-mantle boundary with this complex thermal gradient in between. It is this non-uniform temperature distribution in the horizontal direction that drives the flow in the mantle which eventually becomes unstable because of the rock weakening mechanisms. The horizontal temperature gradient in the upper boundary layer produces flow toward the center of the domain which causes the middle part of the boundary layer to thicken. Eventually this middle part of the boundary layer becomes gravitationally unstable, and runaway of a cold blob of rock that had been in that boundary layer ensues.

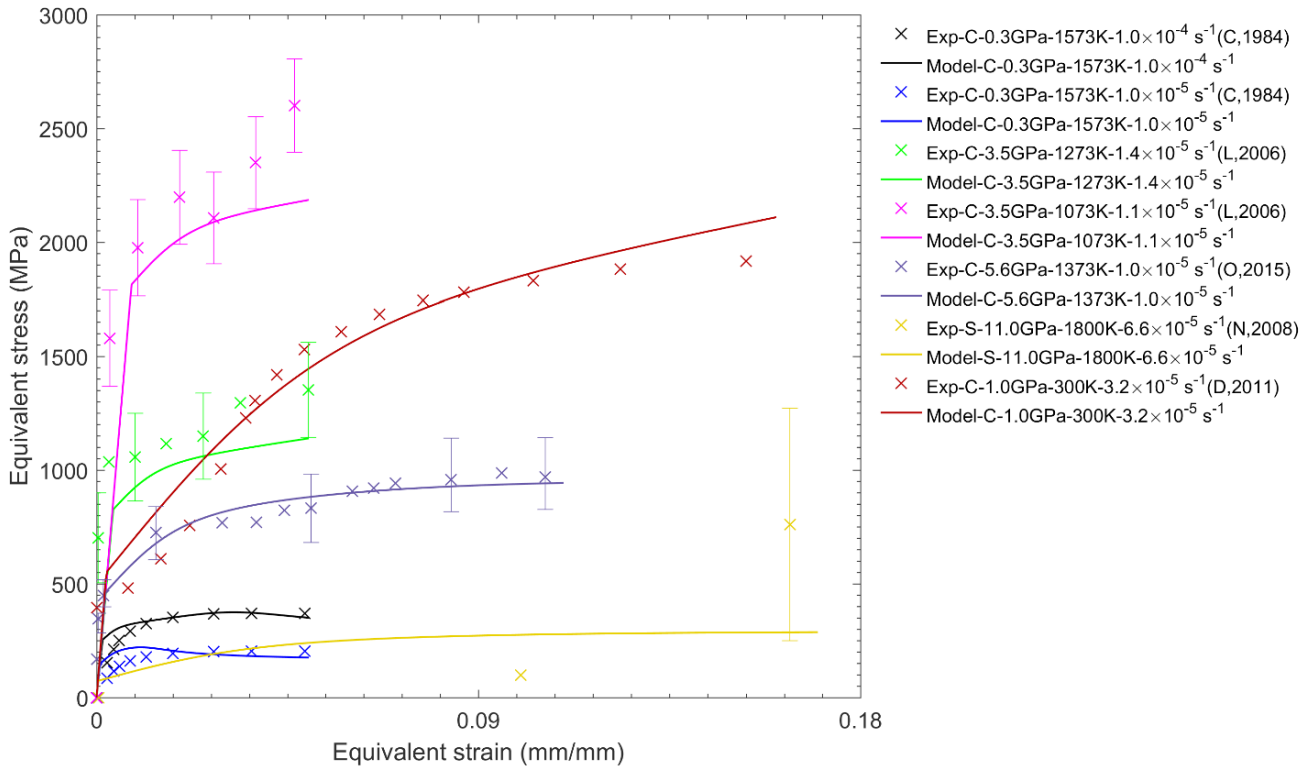

Figure 4. Plot for experimental stress-strain curves (marks) of olivine and their calibrated results (solid lines) at various temperatures, pressures, strain rates, and stress states, using the ISV model constants (summarized in Table 1). The error bars show the uncertainty of each experimental datum. The ISV model fits most of the experimental data within its uncertainty range. In the legend, C and S represent uniaxial compression and shear (torsion) deformation, respectively. The next numbers with 'GPa' and 'K' indicate the pressure and temperature in each experiment, respectively. The next number with 's^{-1}' indicates the applied strain rate. Using this calibrated ISV model for olivine, TERRA calculates realistic mechanical properties at various temperatures, pressures, strain rates, and stress states. C,1984: Chopra and Paterson (1984); L,2006: Li *et al.* (2006); O,2015: Ohuchi *et al.* (2015); N,2008: Nishihara *et al.* (2008); D,2011: Druiventak *et al.* (2011).

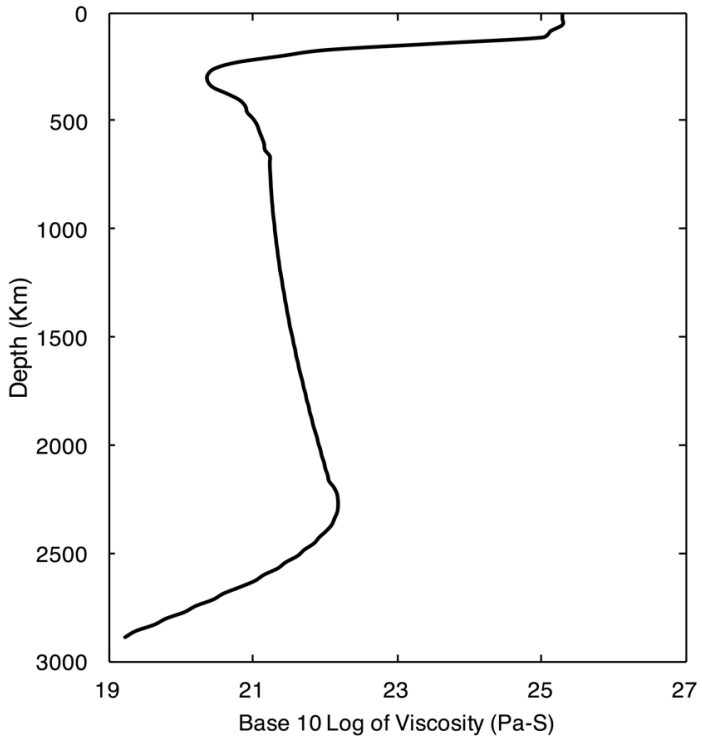

Figure 5. Plot for the initial viscosity profile throughout the mantle's depth in TERRA. The reference viscosity η_0 is 23 in base 10 log scale. Based on Eq. (19), the pressure and temperature dependent initial viscosity profile was generated before the simulation starts.

Table 1. Calibrated ISV model constants and parameters.

	Constants	Values		Constants	Values		Constants	Values
Yield Stress	C1 (MPa)	9.014e+03	*Pressure sensitivity*	C21 (K·MPa^{-1})	2.358e–01	*Grain*	E_g^* (J·mol^{-1})	5.254e+05
	C2 (K)	8.875e+03		C22	0.000e+00		V_g^* (m^3·mol^{-1})	3.000e–06
	C3 (MPa)	1.559e–02		C23 (K·MPa^{-1})	4.331e–02		Cx7 (μm·s^{-Cx8})	6.500e+05
	C4 (K)	1.044e+04		C24 (K·MPa^{-1})	7.952e–01		Cx8	2.500e–01
	C5 (s^{-1})	1.000e–05		C25	0.000e+00		Cx9 (μm^{-2})	1.000e+00
	C6 (K)	0.000e+00		C26 (K·MPa^{-1})	1.000e–03		z	8.000e–01
	C19 (K^{-1})	0.000e+00	*Stress state*	Ca	-5.500e–01		a	7.400e+00
	C20 (K)	0.000e+00		Cb	0.000e+00		b	5.300e+00
Kinematic hardening $\dot{\vec{\alpha}}$	C7 (MPa^{-1})	1.944e+03	*Recrystalliazation*	Cx1 (MPa^{-1})	1.000e–01			
	C8 (K)	5.999e+04		Cx2 (K)	5.000e+02			
	C9	2.964e–02		Cdp (K·MPa^{-1})	2.000e–01			
	C10	0.000e+00		Cx3 (MPa^{-1}s^{-1})	1.000e–01			
	C11 (MPa^{-1}·s^{-1})	4.230e–02		Cx4 (K)	1.000e+03			
	C12 (K)	1.518e+04		Csp (K·MPa^{-1})	2.500e+00			
Isotrophic hardening $\dot{\kappa}$	C13 (MPa^{-1})	3.626e+01		Cx5	3.000e+00			
	C14 (K)	1.135e+03		Cx6 (K)	5.000e+02			
	C15	1.727e–01		Cxa	6.000e–01			
	C16	0.000e+00		Cxb	1.000e+00			
	C17 (MPa^{-1}·s^{-1})	9.309e+06		*n*	4.000e+00			
	C18 (K)	1.728e+05		k_0 (μMn·s^{-1})	1.930e+18			

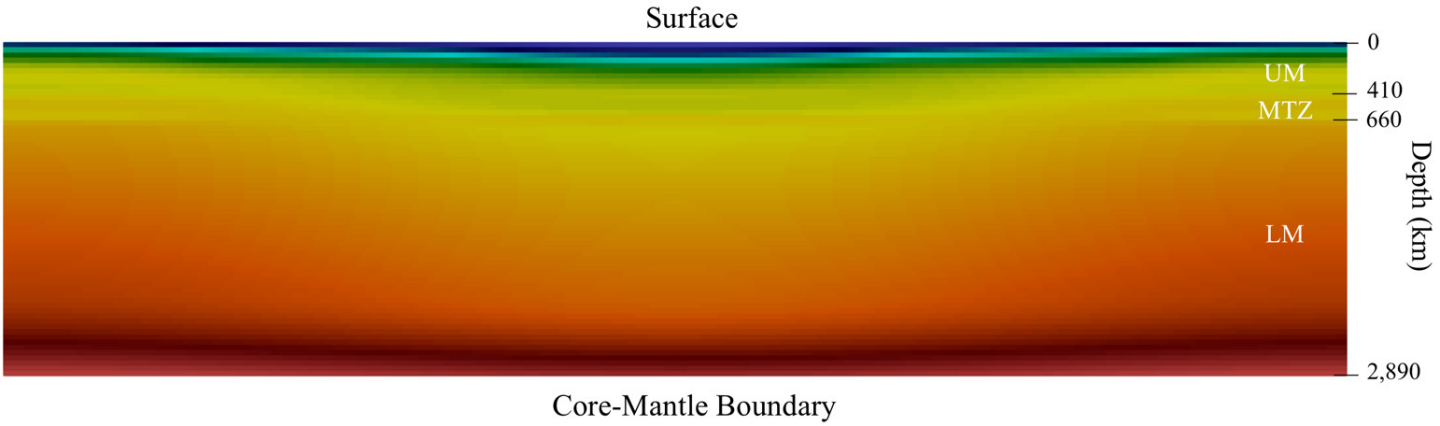

Figure 6. Representation of the Earth's mantle initial temperature structure in TERRA2D. Boundary temperatures are fixed at 300 K at the top boundary and 3700 K at the bottom boundary. Laterally, temperatures vary in accord with a single period of the cosine function except at the boundaries. UM, MTZ, and LM represent the upper mantle, the mantle transition zone, and the lower mantle, respectively.

RESULTS AND DISCUSSIONS

1. Mechanical effects of weakening mechanisms

Once the cold blob of rock begins to sink, an increasing amount of mechanical energy is dissipated as heat in the volume surrounding the blob; consequently, the temperature within the envelope surrounding the blob increases (Fig. 7) as first explained by Baumgardner (2003). This increased temperature near the blob also influences the microstructural features. First of all, the increased annihilation of dislocations weakens the rock near the blob. Second, the grain size of surrounding rock of the blob increases because of the increased temperature from the shear heating (Fig. 8). As the grain size increased, the interaction between dislocation and grain boundary decreases, which also leads to weakening. Therefore, the reduced strength of the rock surrounding the blob contributes strongly to the runaway process.

Noteworthy is the fact that the downwelling blob's grain size decreases to approximately 5 μm as a result of strong deformation combined with dynamic recrystallization under cold temperature. However, average grain size of the leading part of downwelling blob remains at approximately the initial value of 100 μm. This occurs because the leading part of the blob does not undergo large deformations due to its high strength (and high viscosity) because of its relatively colder temperature and the extremely high pressure. In essence, it acts like a penetrator moving hydrodynamically through a thick viscous target.

The most prominent mechanism that operates in the upper mantle is that of recrystallization. There the recrystallized volume fraction (i.e., the dislocation free volume fraction) increases to about 87%; this dramatic reduction of the dislocation density (see Fig. 9) leads to strong weakening. In particular, the rock surrounding the descending blob and the blob itself undergoes a large amount of the dynamic recrystallization. The reason for the absence of recrystallization in the transition zone and lower mantle, possibly may be attributed to the extrapolation that we were required to make beyond the limited pressure and temperature ranges provided in the available experimental data. Several experimental studies at high pressures and temperatures report the occurrence of recrystallization during deformation, although these results are largely qualitative at this point (e.g., Farla et al. 2015). A model for the recrystallization in the deep mantle is therefore an important future objective.

One more important microstructural process that caused a high level of strength weakening was development of texture, or deformation-induced CPO, which is related to plastic grain rotations (plastic spin). Under a shear-dominated stress state, the texture can be highly developed, causing strong weakening of solid rock. The shear-dominated stress occurs around the downwelling blob as shown in the plots of the spin tensor and shear strain (Fig. 10). Therefore, the rock surrounding the blob was weakened additionally by the texture effect as we calibrated the shear stress-strain behavior against the compression stress-strain behavior (see Fig. 4).

Fig. 11 shows the snapshots of plastic strains developed during the simulation. The heterogeneous degree of deformation (thus, heterogeneous microstructures) in the sinking blob can also be readily observed from the plastic strain. This result implies that the mantle's physical properties and its microstructures would be very heterogeneous near the core-mantle boundary where the descending blob arrived. In fact, the seismic data from the earth's interior have shown that strong heterogeneity currently exists near the mantle's base, a region known as D″. In addition, in the simulation most of the lower mantle was deformed only up to 0.5 plastic strain, which is a very small strain compared to that of the upper mantle. However, from an observational standpoint, a remarkably small amount of anisotropy throughout the lower mantle has been found in seismic investigations (Montagner and Kennett 1996), which implies a small degree of plastic deformation (and texture development). Even though more thorough studies are needed, these lines of observational evidence appear to match the simulated results of the present study reasonably well.

The cooperative effects on strength weakening are clearly observed in the kinematic hardening, isotropic hardening, stress, and viscosity (Fig. 12) in our simulations. As shown in these stress and viscosity snapshots, the rock surrounding the sinking blob displays very low stress and viscosity values. An interesting feature in the stress and viscosity plots is the presence of distinct low viscosity bands. These low viscosity bands imply that the entire mantle feels the effects of the runaway instability that produces a catastrophic

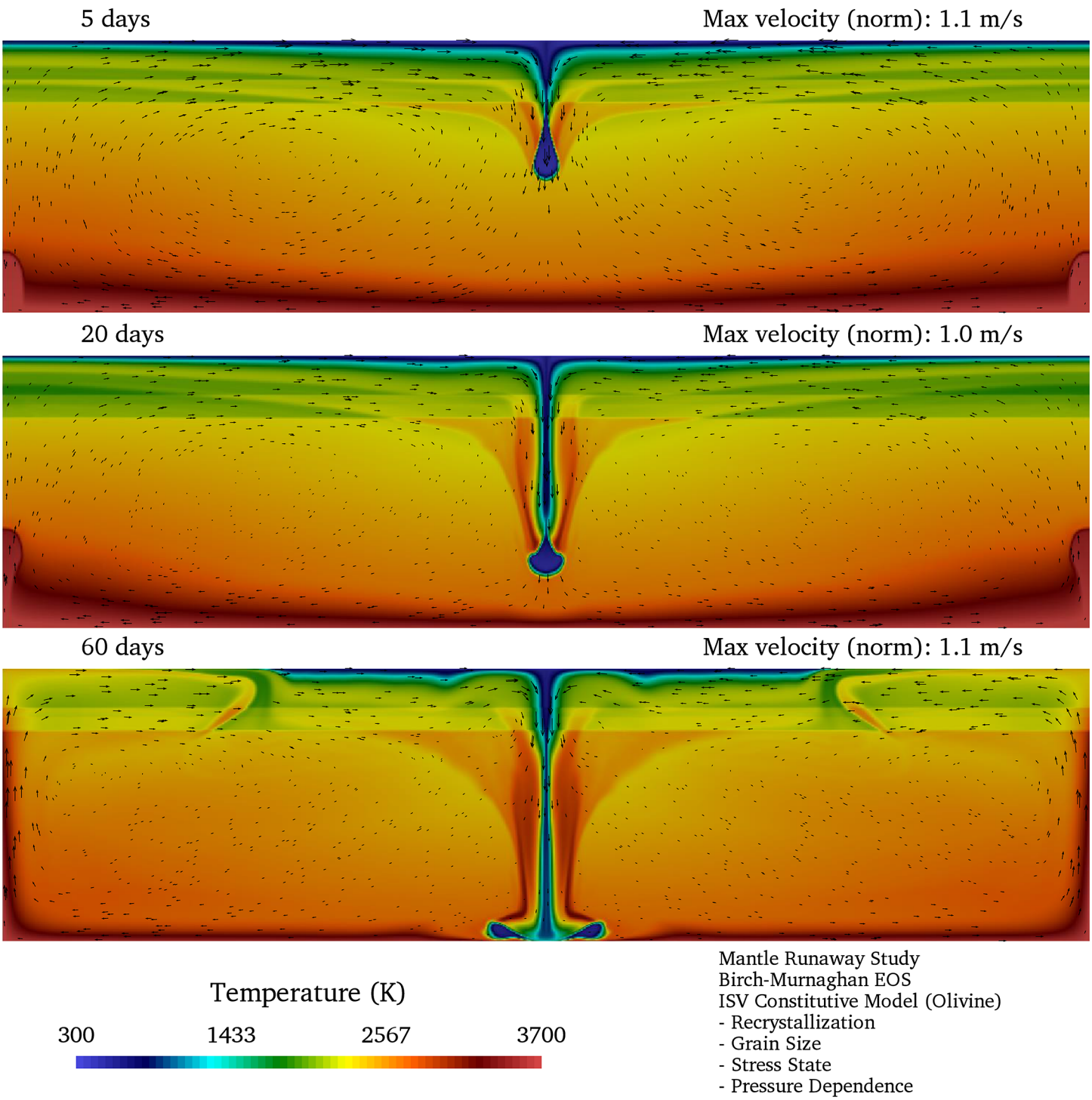

Figure 7. Temperature snapshots from the TERRA2D simulation at the times of 5 days, 20 days, and 60 days after the Flood started. The arrows show the velocity fields of mantle flow. Initially, the cold blob rapidly descended with the maximum velocity of 1.1 m/s. As the gravitational potential energy decreases with time, the mantle's downwelling velocity decreases due to the reduction of the driving force from the gravitational potential energy. At the top surface, the ascending plume pushes the cold dense rock toward the downwelling zone. Note that the increase in the temperature around the descending blob due to the shear (or frictional) heating. The shear heating decreases the viscosity of rock (see Figure 12) leading to the catastrophic runaway process.

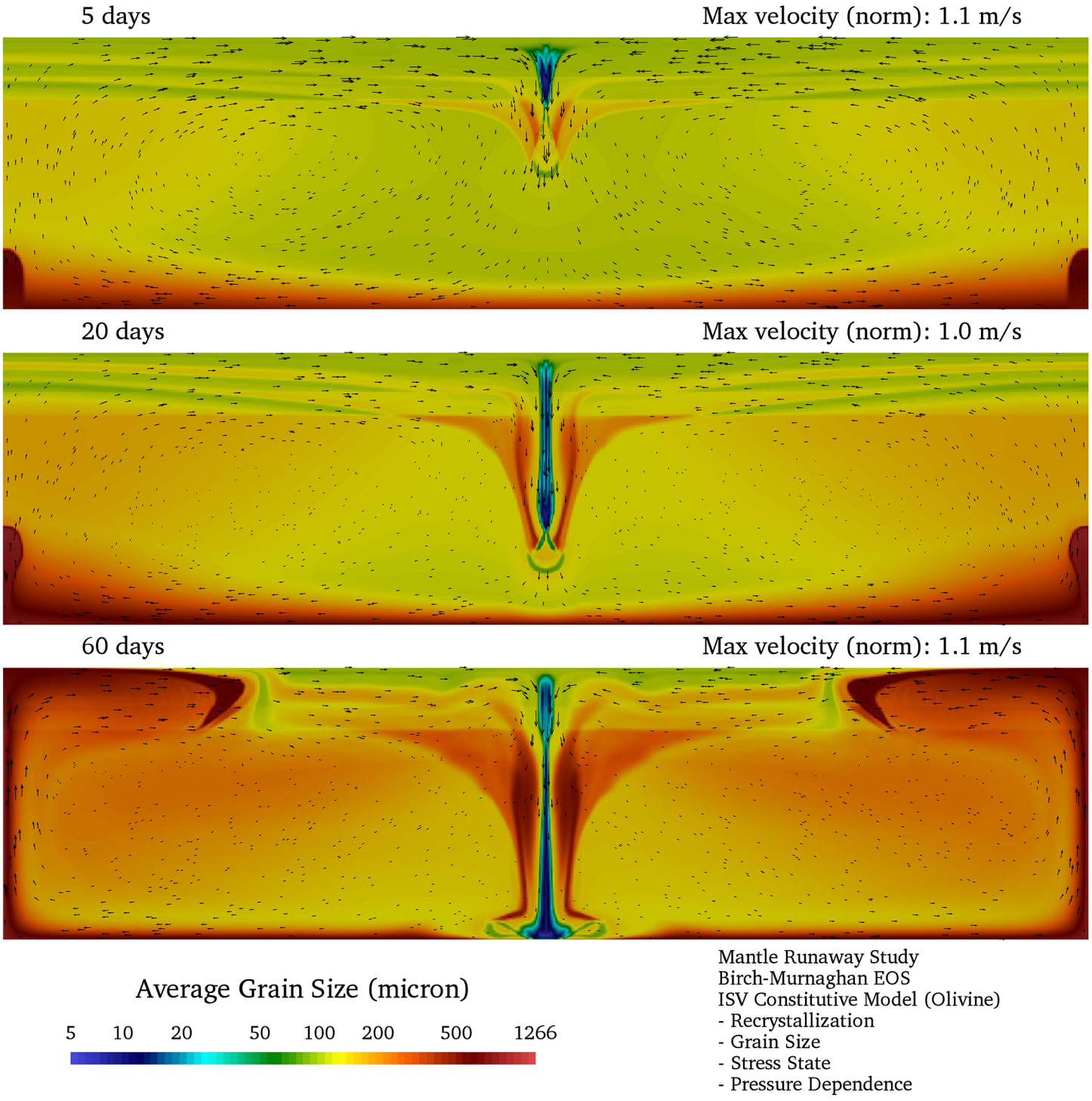

Figure 8. Average grain size snapshots at the times of 5 days, 20 days, and 60 days. The grain growth highly took place due to the shear heating in the surrounding rock of sinking slab. In contrast, the grain size inside of slab was highly reduced (down to 5 μm from the initial grain size 100 μm) due to the dynamic recrystallization. Since the sinking slab was deformed under relatively cold temperature, the grain refinement was dominated.

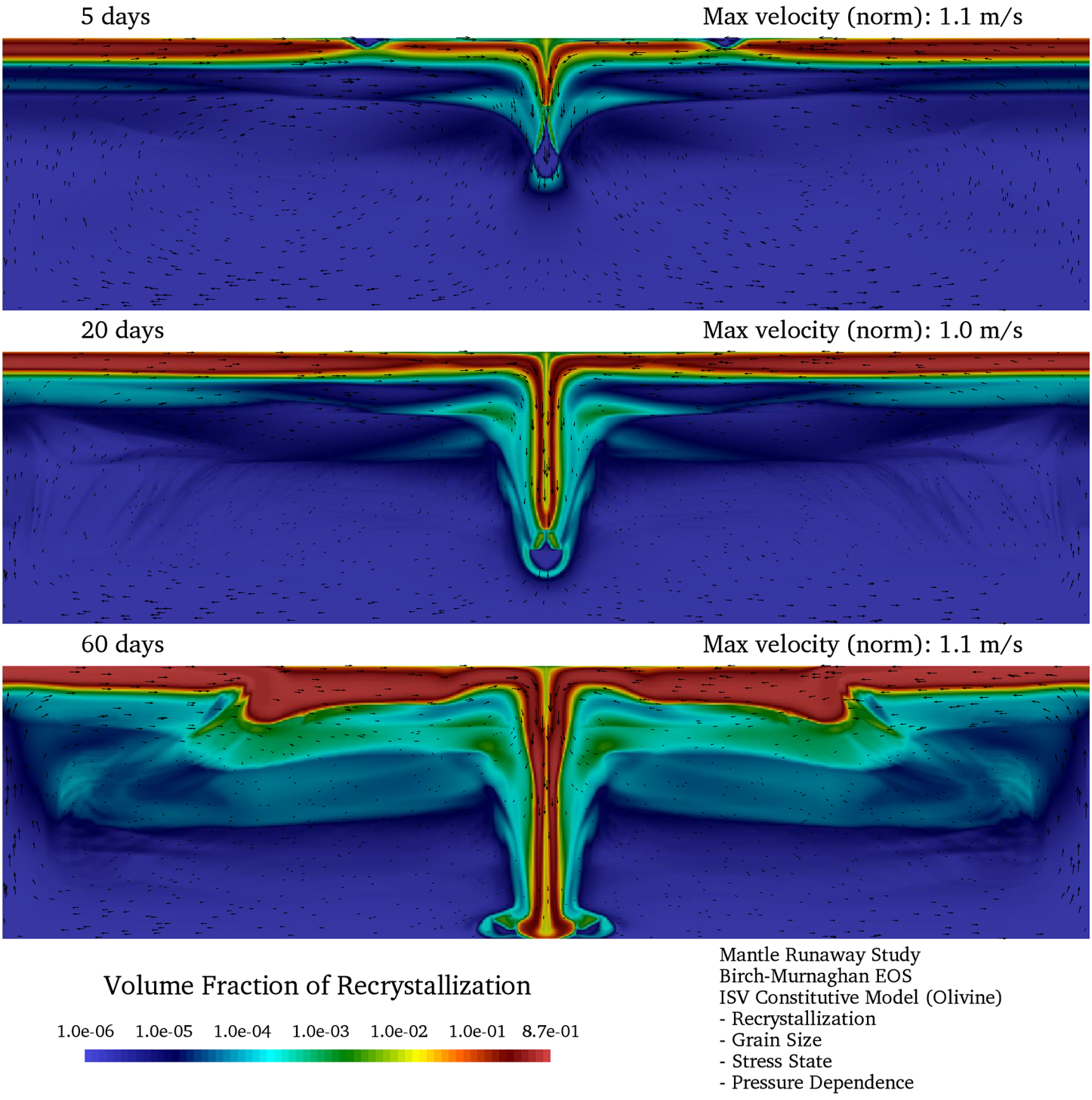

Figure 9. Snapshots of the recrystallized volume fraction at the times of 5 days, 20 days, and 60 days. The volume fraction of dynamic recrystallization was high in regions where the deformation was larger. Most of the upper mantle was highly recrystallized since the recrystallization kinetics was more sensitive to temperature than pressure. By contrast, only little of the lower mantle was recrystallized because the recrystallization was suppressed by high pressure.

mantle overturn.

For this work the ISV model was implemented with the associated microstructural features successfully into the TERRA3D code making 3D simulations possible. Figs. 14-18 show the temperature, stress, average grain size, viscosity, and plastic strain, respectively, of an illustrative simulation. Just as in the 2D simulation, extreme strength weakening due to effects of recrystallization, grain size, and texture were observed. Strong mechanical and microstructural heterogeneities produced by the cold material that descended catastrophically from the upper boundary was also observed at the core-mantle boundary. Most notably, the low viscosity bands present in the 2D calculation were also clearly evident in this 3D case, even though the grid resolution was not that high in the radial direction. These low viscosity bands revealed that the entire mantle participated in the catastrophic runaway event.

2. Comparison of weakening mechanisms

Finally, we have undertaken a limited study to compare the relative importance of three of the strength weakening mechanisms: recrystallization (REX), grain size (GS), and texture (SS). Fig. 13 summarizes the results of four comparison cases: 1) REX, GS, and SS; 2) REX and GS; 3) REX and SS; and 4) GS and SS. Fig. 13 displays snapshots at a time of 30 days of the base 10 log of the norm of stress.

To summarize the findings, without any of these three microstructural mechanisms, the mantle still shows a tendency to overturn in the catastrophic manner due to the shear heating and the recovery process as shown in the previous studies of Baumgardner (2003) and Sherburn (2013). However, with the three mechanisms, the strength of mantle is reduced even more. When the texture effect is turned off (Case #2), the overall mantle strength increases significantly such that the maximum flow velocity decreases by almost half. By comparison, the grain size and recrystallization mechanisms appear to have much smaller effects, but they nevertheless reduce rock strength in localized regions such as in the upper mantle and mantle near the cold descending blob.

As discussed earlier, our recrystallization treatment in the transition zone and the lower mantle is limited in its realism by the lack of experimental data. In addition, our treatment of grain size dependence on rock strength, particularly for grain size sensitive mechanisms (i.e., weakening mechanisms when the grain size is small) such as diffusion creep and grain boundary sliding, needs improvement. The present model focuses primarily on the interactions between grain boundary and dislocations without deep consideration of the grain size sensitive mechanisms. When the grain size is significantly decreased by dynamic recrystallization, these grain size sensitive mechanisms might conceivably produce much more weakening than our present results indicate.

In spite of these limitations, our preliminary study of weakening

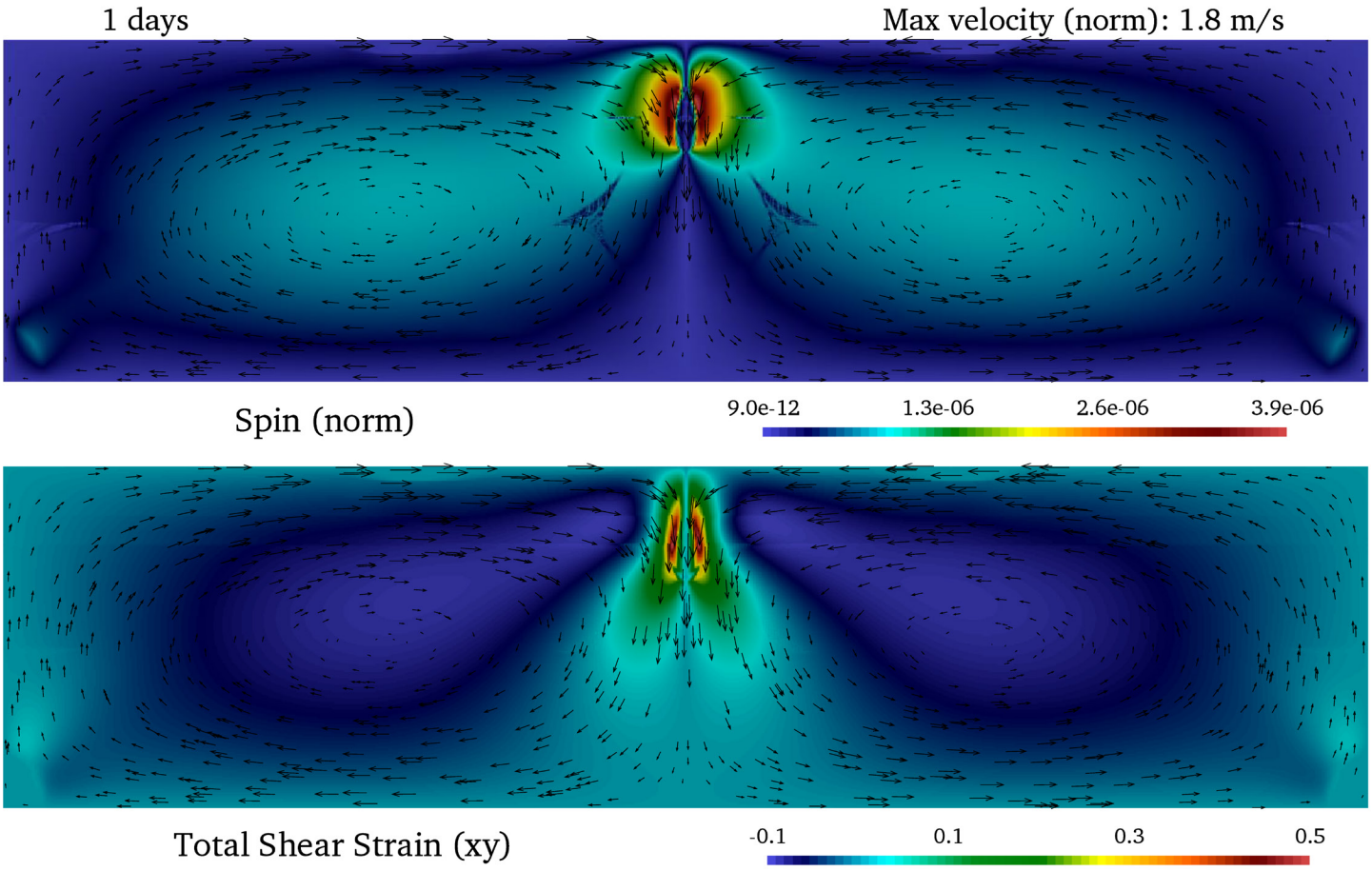

Figure 10. Snapshots of norm of spin tensor (or vorticity) and total shear strain (*i.e.*, sum of elastic and plastic shear strain) at the first day. Both of the spin and shear strain were very high around the descending slab. From these snapshots, it is clearly shown that the surrounding rock of slab underwent high shear deformation by plastic spin.

mechanisms suggests that the texture effect, which arises from plastic grain rotations, plays a larger role than recrystallization and grain size role in reducing rock strength in most circumstances.

FUTURE WORK

From this study, the TERRA simulations demonstrated that the effects of grain size, recrystallization, and deformation-induced texture on the weakening of mantle rock strength are important and almost certainly played a notable role in the mantle dynamics responsible for the Genesis Flood. Nevertheless, our current model has major limitations. First of all, a multi-mineral composition treatment is urgently needed as we only used olivine. Our current treatment relies exclusively on the measured microstructural and mechanical properties of olivine. Since olivine exists only in the upper mantle, its microstructural and mechanical behavior cannot adequately represent the whole mantle. A multiphase model that reflects the mantle's actual mineralogical composition and whose complete suite of microstructural parameters are derived from solid

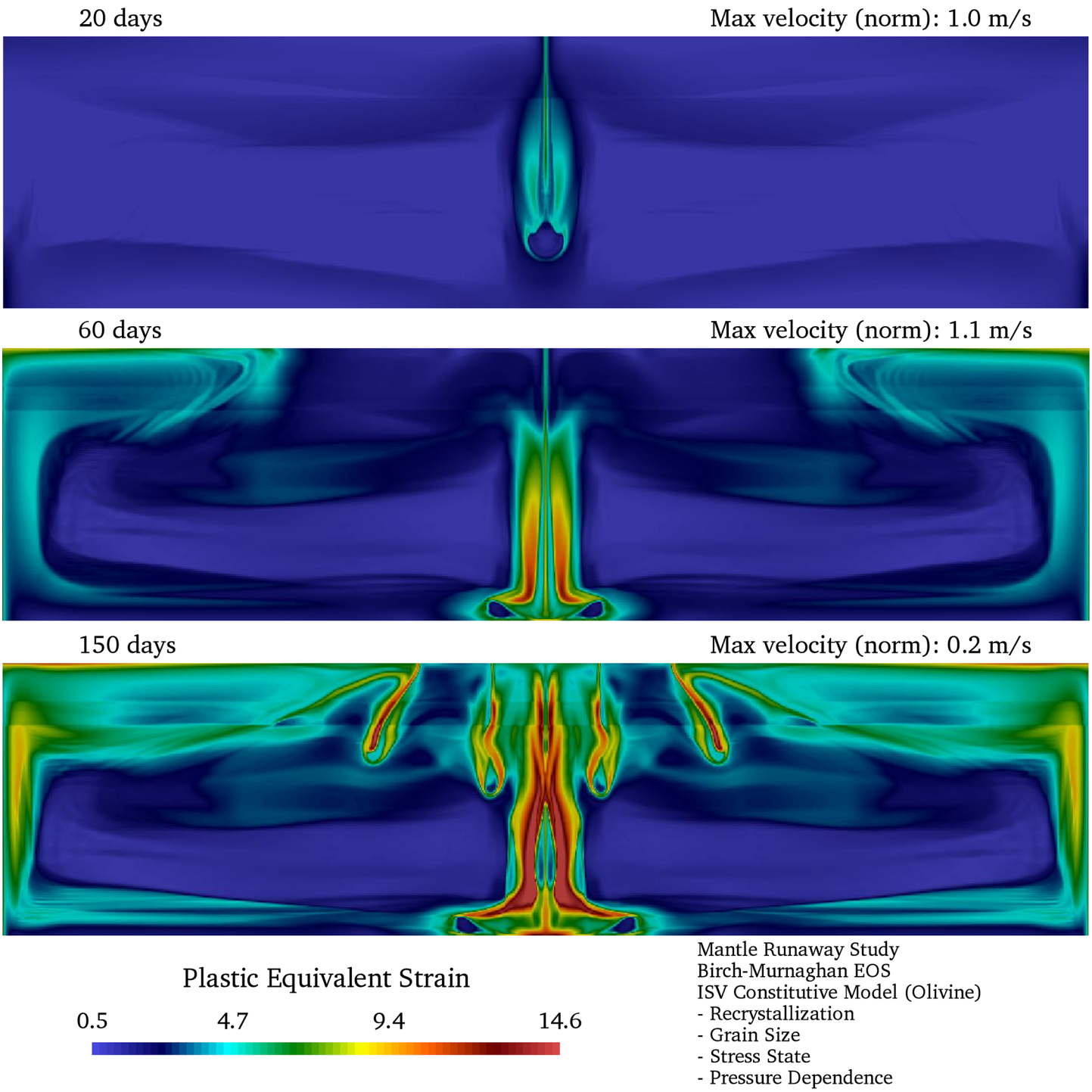

Figure 11. Snapshots of the plastic equivalent strain at the times of 20, 60, and 150 days. Deformation in descended slab is highly heterogeneous; therefore, the microstructures of slab may be also very heterogeneous. In addition, overall lower mantle was rarely deformed compared to the upper mantle.

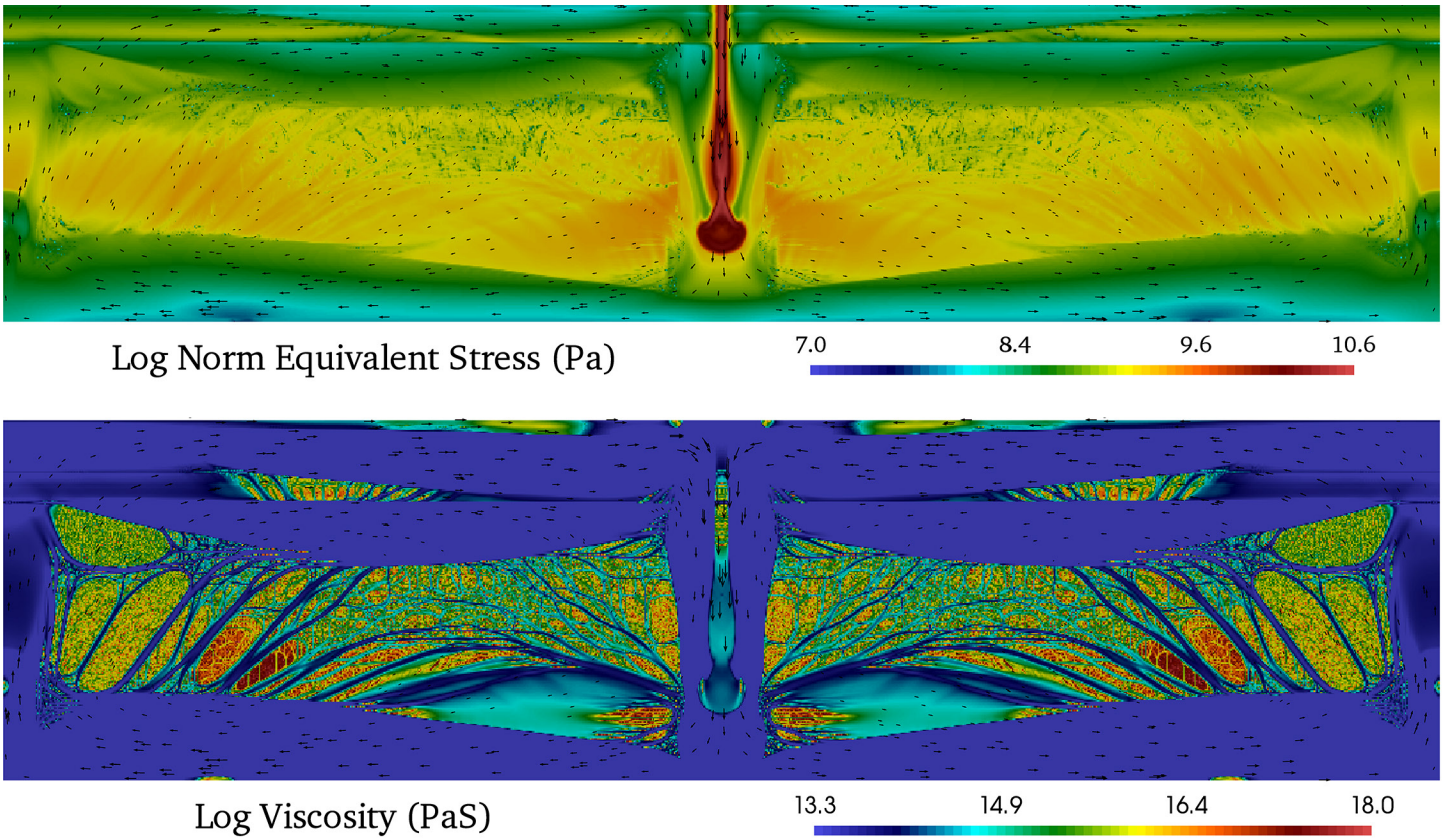

Figure 12. Snapshots of the equivalent stress and viscosity in the base 10 logarithmic scale at the time of 20 days. Due to high strain rate, the viscosity of the entire mantle was significantly decreased from the initial reference viscosity that is comparable to the one of present day. Also, many low viscosity bands were observed. Because of the high pressure, the strength and viscosity in most of lower mantle were higher than in the upper mantle.

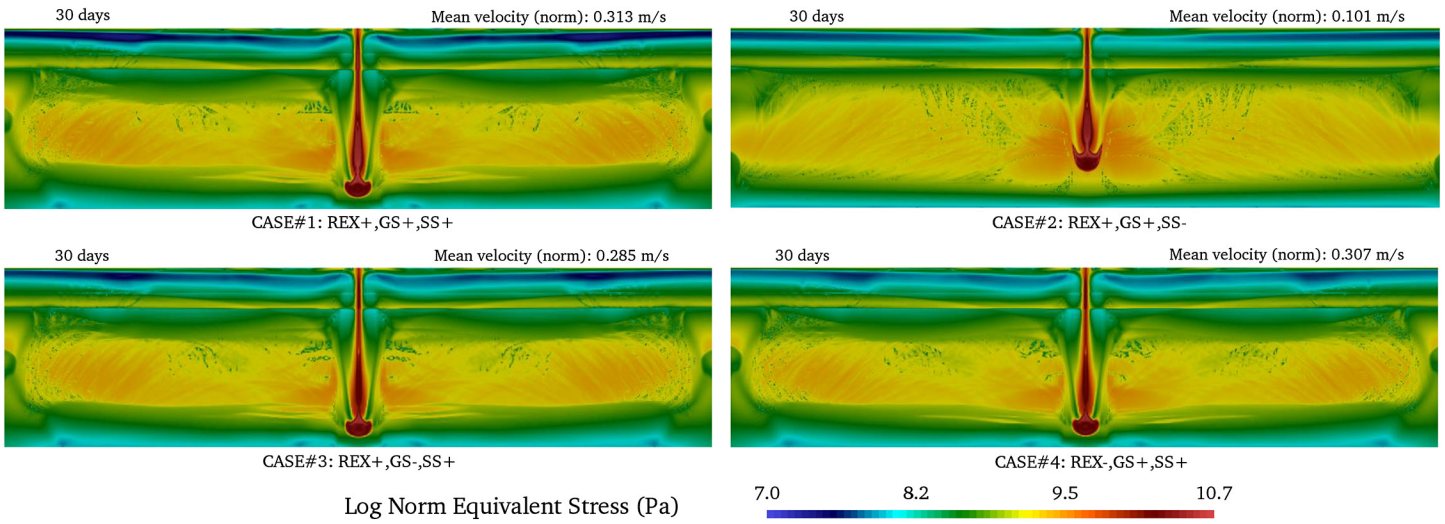

Figure 13. Comparison of the strength at the 30th day. In order to compare contributions of effect of each mechanism (recrystallization (REX), grain size (GS), and texture (SS)), we ran four simulations of different cases. The positive sign represents effect of that mechanism was turned on in that case. When the texture (plastic spin) effect was turned off, the maximum mantle flow velocity was decreased by almost half. From these preliminary case studies, this paper concludes that texture effect was the most significant in weakening the overall mantle rock strength.

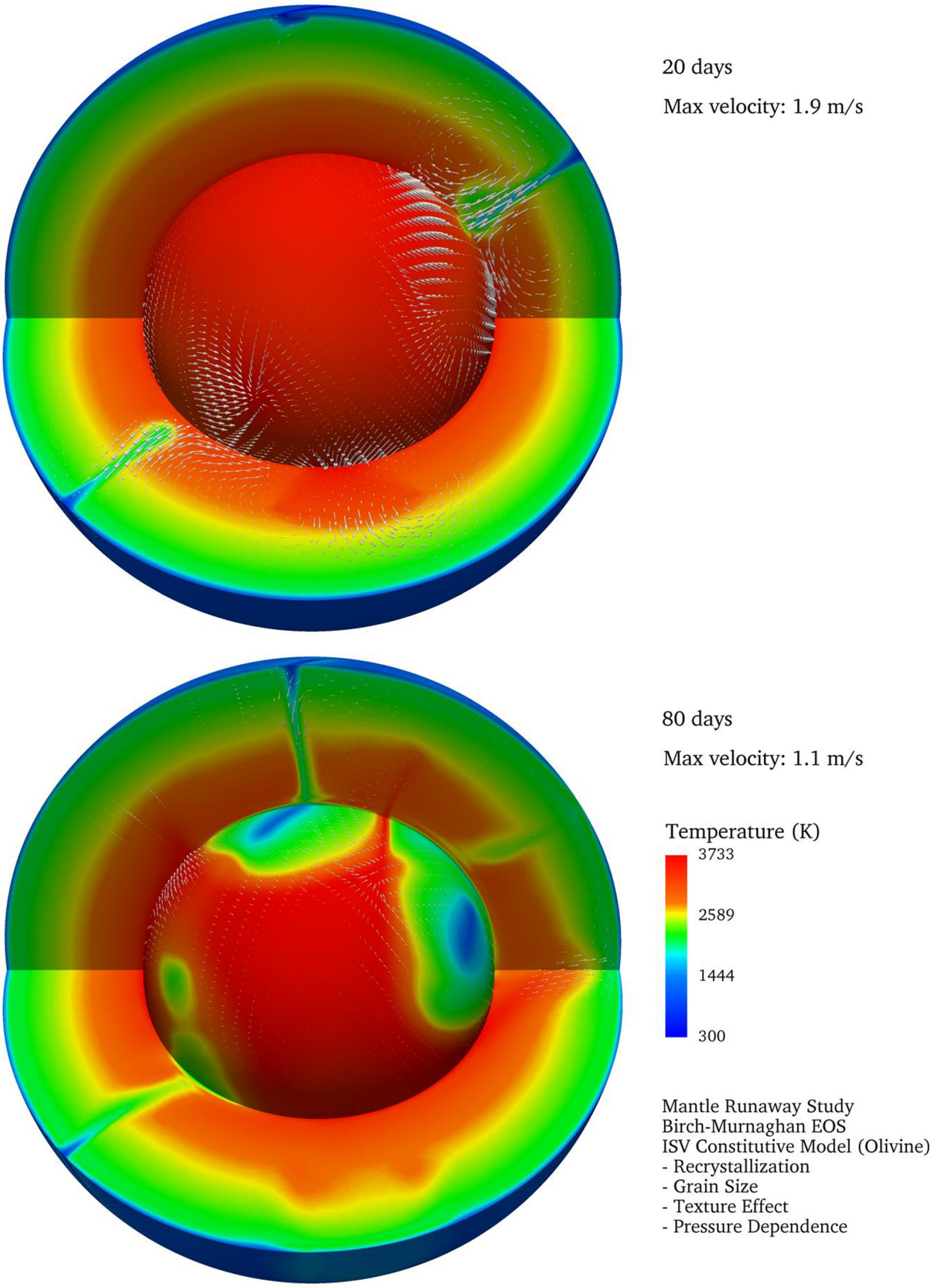

Figure 14. Temperature plots of TERRA3D simulation with the present ISV constitutive model at the times of 20 and 80 days. Note that the rapidly descending cold dense slab from the top surface.

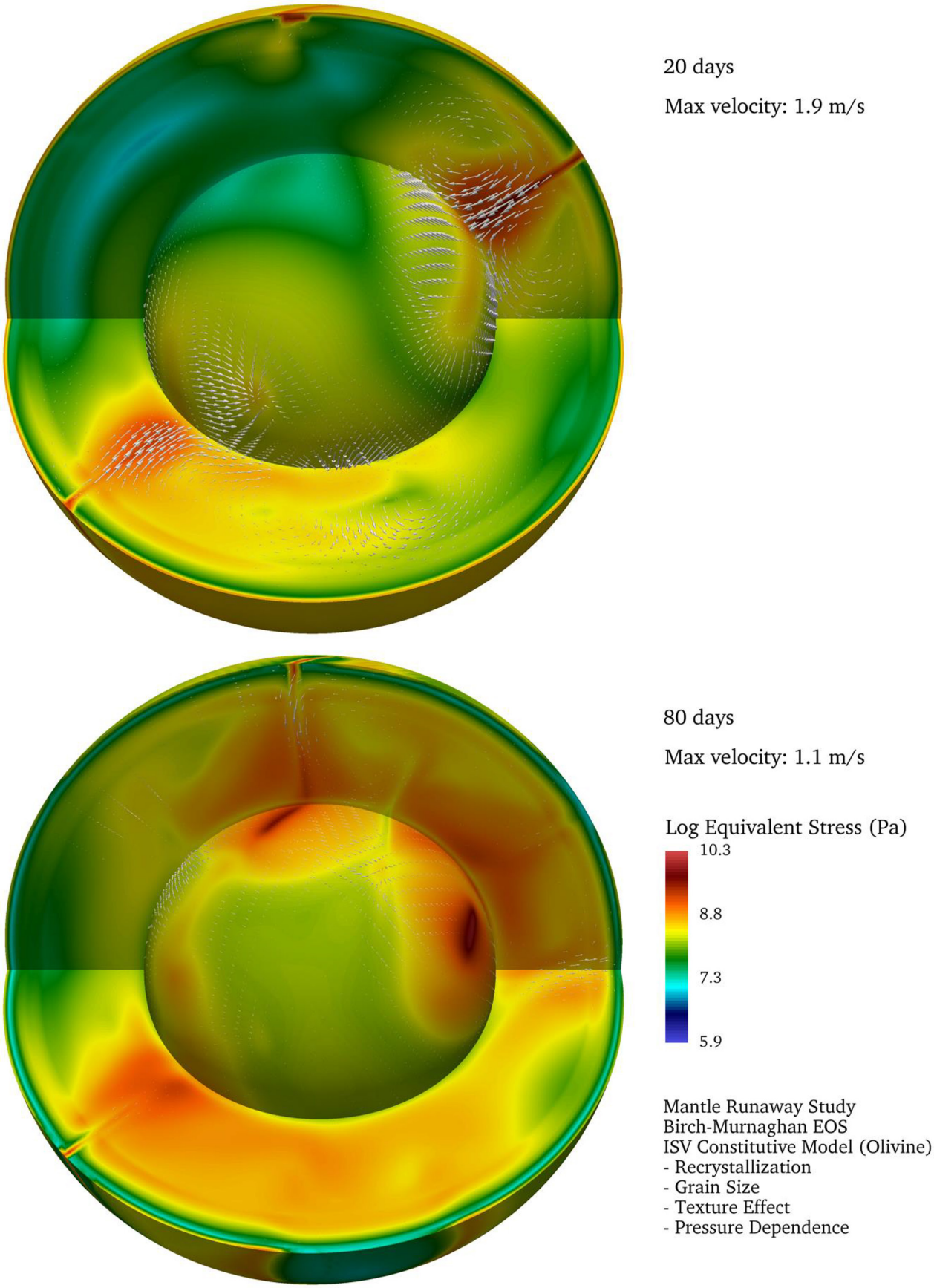

Figure 15. Equivalent stress plots from the TERRA3D simulation in the base 10 logarithmic scale at the times of 20 and 80 days. Highly hardened slab was deflected at the core-mantle boundary.

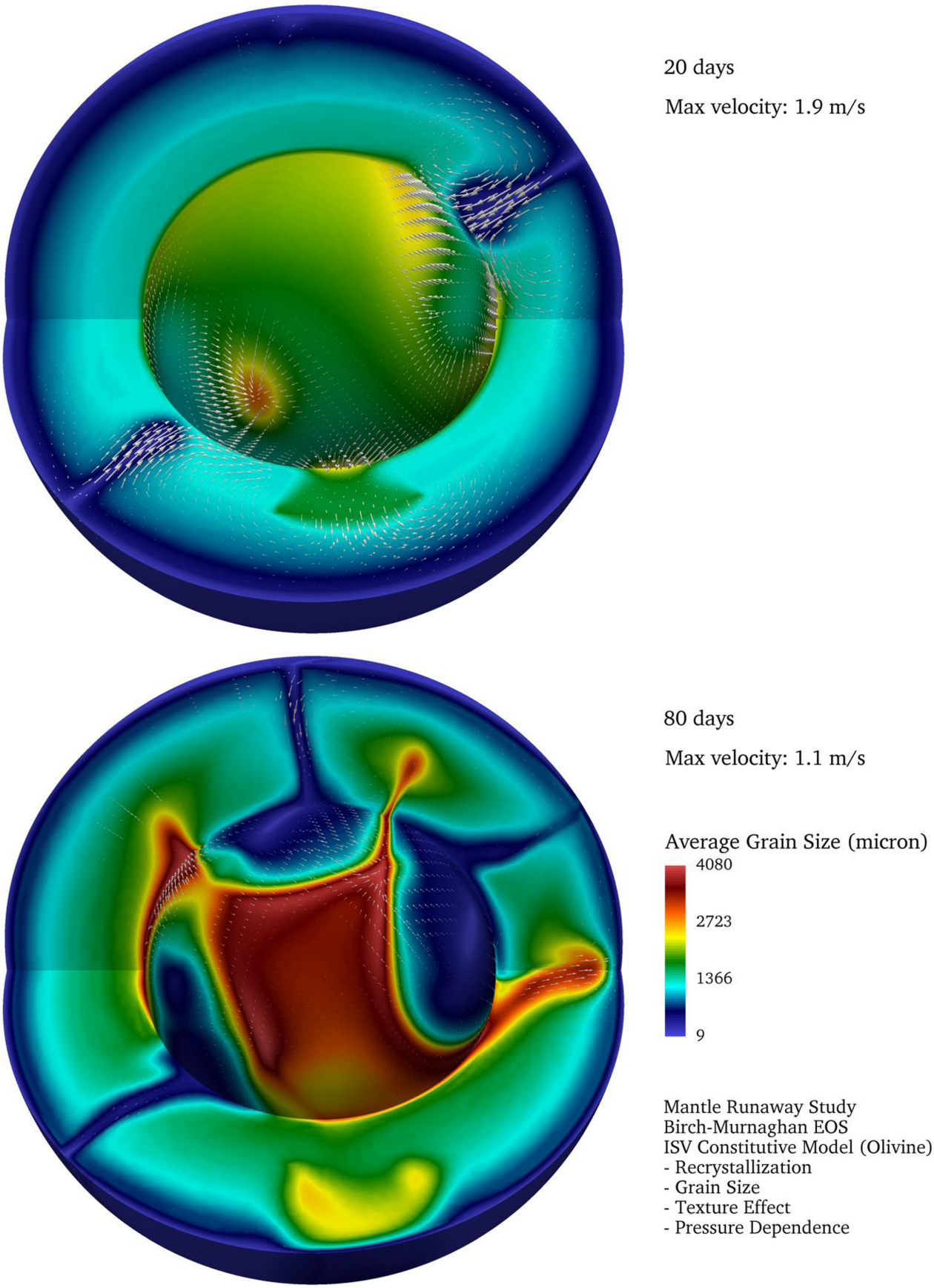

Figure 16. Average grain size plots from TERRA3D simulations at the times of 20 and 80 days. Note the descended rock with highly refined grains by the dynamic recrystallization at the core-mantle boundary.

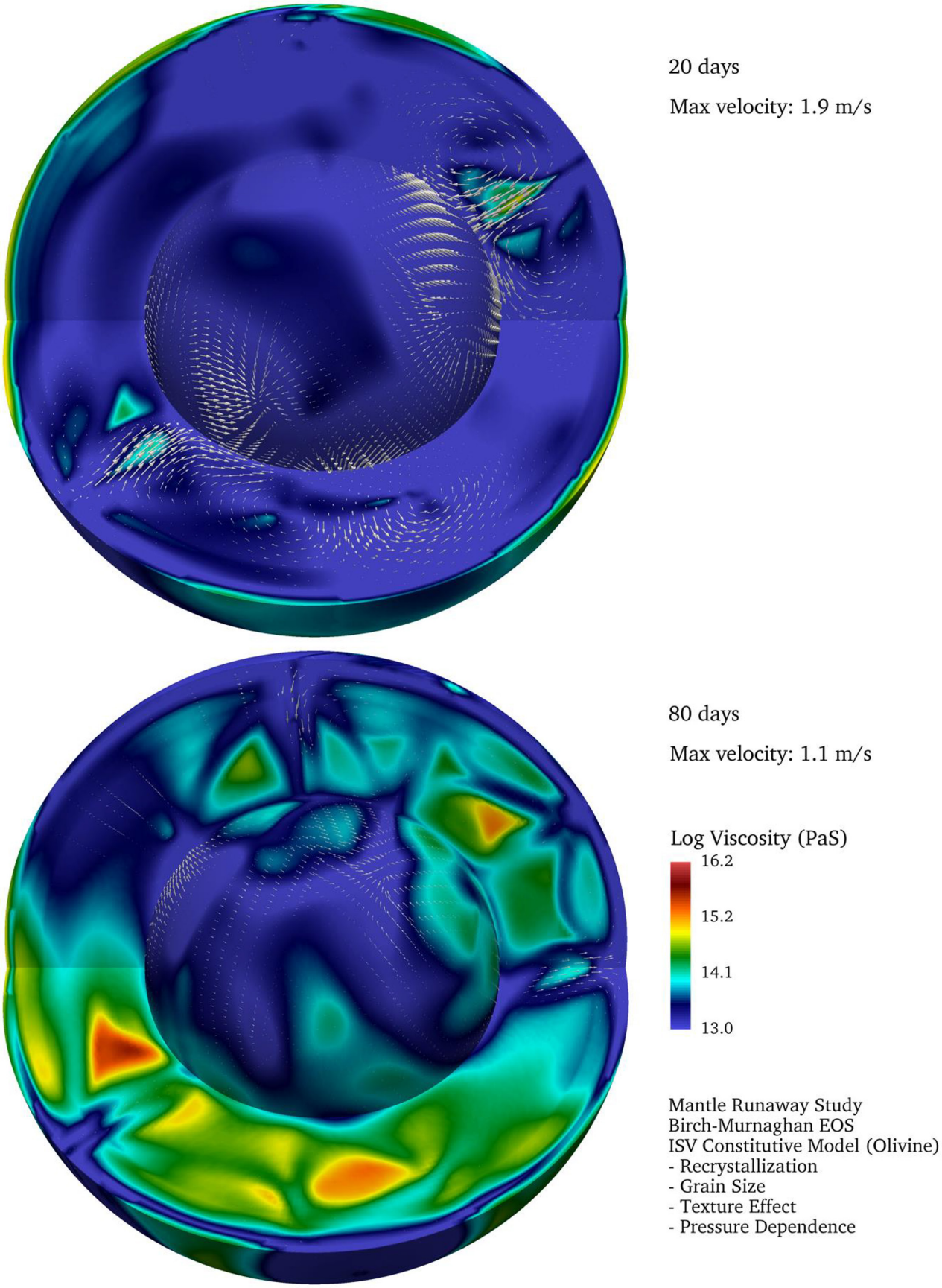

Figure 17. Viscosity plots from the TERRA3D simulation in the base 10 logarithmic scale at the times of 20 and 80 days. The low viscosity bands that may play a role in increasing convection rate were also observed.

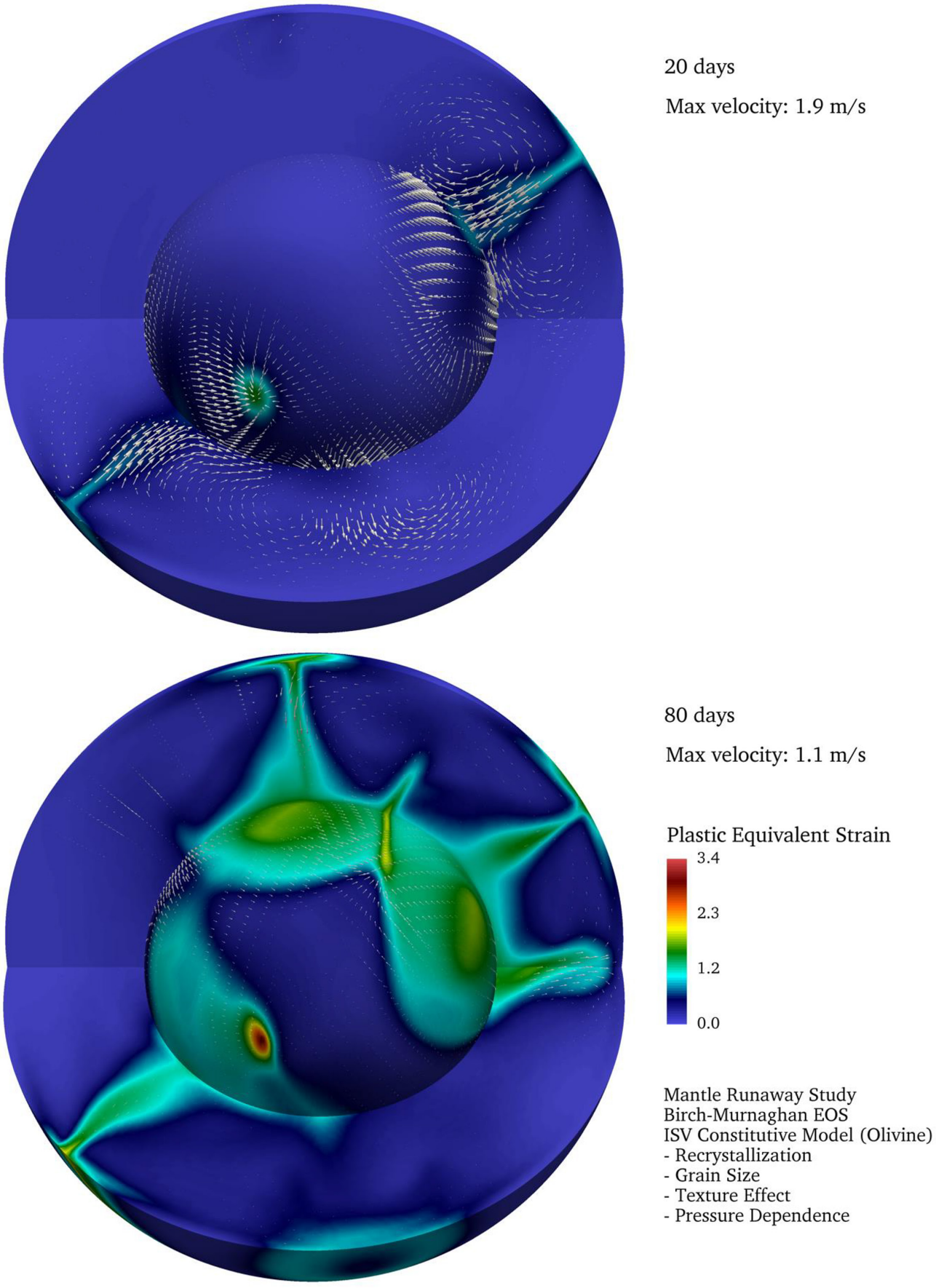

Figure 18. Plots for the plastic equivalent strain from the TERRA3D simulation at the times of 20 and 80 days.

experimental and seismological investigations is clearly the goal for this type of high fidelity geodynamic model.

CONCLUSIONS

In this paper, we have improved the constitutive model for rock deformation by adding the structure-property relations in order to explore the mantle dynamics associated with the Genesis Flood. In particular, effects from grain size, recrystallization, and deformation induced texture were included. Our efforts are motivated by our conviction that the Biblical account of the Genesis Flood is genuine history. The TERRA results that use an improved rock deformation model clearly affirm earlier work that indicated the mantle's inherent potential for runaway catastrophic overturn. This potential for the mantle instability arises from the extreme weakening behavior resulting from the relationship between microstructural features (herein texture, recrystallization, and grain size) and thermomechanical properties (e.g., stress and viscosity) under the conditions of temperature, pressure, and strain rate within the mantle during the Genesis Flood. This work demonstrates that this potential is genuine and thereby provides strong support the historicity of Genesis Flood as a global catastrophic event.

REFERENCES

Austin, S.A., J.R. Baumgardner, D.R. Humphreys, A.A. Snelling, L. Vardiman, and K.P. Wise. 1994. Catastrophic plate tectonics: A global Flood model of earth history. In *Proceedings of the Third International Conference on Creationism*, ed. R.E. Walsh, pp. 609–621, Pittsburgh, PA: Creation Science Fellowship.

Bammann, D.J. 1990. Modeling temperature and etrain rate dependent large of metals. *Applied Mechanics Reviews* 43, no. 5:312-319 [Part 2].

Bammann, D.J., M.L. Chiesa, M.F. Horstemeyer, and L.I. Weingarten. 1993. Failure in ductile materials using finite element methods. *Structural Crashworthiness and Failure*, eds. T. Wierzbicki, and N. Jones, pp. 1-54. Elsevier Applied Science, The Universities Press (Belfast) Ltd.

Baumgardner, J.R. 1986. Numerical simulation of the large-scale tectonic changes accompanying the Flood. In *Proceedings of the First International Conference on Creationism*, Volume II, eds. R.E. Walsh, C.L. Brooks and R.S. Crowell, pp. 17-30. Pittsburgh, Pennsylvania: Creation Science Fellowship.

Baumgardner, J.R. 1994. Computer modeling of the large-scale tectonics associated with the Genesis Flood. In *Proceedings of the Third International Conference on Creationism*, ed. R.E. Walsh, pp. 49–62. Pittsburgh, PA: Creation Science Fellowship.

Baumgardner, J.R. 2003. Catastrophic plate tectonics: The physics behind the Genesis Flood. In *Proceedings of the Fifth International Conference on Creationism*, ed. R.L. Ivey, Jr., pp. 113–126. Pittsburgh, Pennsylvania: Creation Science Fellowship.

Brown, A.A., and D.J. Bammann. 2012. Validation of a model for static and dynamic recrystallization in metals. *International Journal of Plasticity* 32–33:17–35.

Chen, J. 2016. Lower-mantle materials under pressure. *Science* 351, no. 6269:122–123.

Chopra, P.N., and M.S. Paterson. 1984. The role of water in the deformation of dunite. *Journal of Geophysical Research: Solid Earth* 89:7861–7876.

Dafalias, Y.F. 2000. Orientational evolution of plastic orthotropy in sheet metals. *Journal of the Mechanics and Physics of Solids* 48:2231–2255.

Derby, B., and M.F. Ashby. 1987. On dynamic recrystallisation. *Scripta Metallurgica* 21:879–884.

Doherty, R.D., D.A. Hughes, F.J. Humphreys, J.J. Jonas, D.J. Jensen, M.E. Kassner, W.E. King, T.R. McNelley, H.J. McQueen, and A.D. Rollett. 1997. Current issues in recrystallization: A review. *Materials Science and Engineering:A* 238:219–274.

Druiventak, A., C.A. Trepmann, J. Renner, and K. Hanke. 2011. Low-temperature plasticity of olivine during high stress deformation of peridotite at lithospheric conditions — An experimental study. *Earth and Planetary Science Letters* 311:199–211.

Dziewonski, A.M., and D.L. Anderson. 1981. Preliminary reference earth model. *Physics of the Earth and Planetary Interiors* 25:297–356.

Farla, R., G. Amulele, J. Girard, N. Miyajima, and S. Karato. 2015. High-pressure and high-temperature deformation experiments on polycrystalline wadsleyite using the rotational Drickamer apparatus. *Physics and Chemistry of Minerals* 42 no. 7:541–558.

Girard, J., G. Amulele, R. Farla, A. Mohiuddin, and S. Karato. 2016. Shear deformation of bridgmanite and magnesiowüstite aggregates at lower mantle conditions. *Science* 351, no. 6269:144–147.

Hall, E.O. 1954. Variation of hardness of metal with grain size. *Nature* 173, 948-949.

Hansen, L.N., M.E. Zimmerman, and D.L. Kohlstedt. 2012. The influence of microstructure on deformation of olivine in the grain-boundary sliding regime. *Journal of Geophysical Research: Solid Earth* 117, B09201.

Hiraga, T., C. Tachibana, N. Ohashi, and S. Sano. 2010. Grain growth systematics for forsterite ± enstatite aggregates: Effect of lithology on grain size in the upper mantle. *Earth and Planetary Science Letters* 291:10–20.

Horstemeyer, M.F., J. Lathrop, A.M. Gokhale, and M. Dighe. 2000. Modeling stress state dependent damage evolution in a cast Al–Si–Mg aluminum alloy. *Theoretical and Applied Fracture Mechanics* 33:31–47.

Horstemeyer, M.F., and D.L. McDowell. 1998. Modeling effects of dislocation substructure in polycrystal elastoviscoplasticity. *Mechanics of Materials* 27:145–163.

Horstemeyer, M.F. 1998. Use of history dependent material models for simulating geophysical events related to the Bible. In *Proceedings of the Fourth International Conference on Creationism*, ed. R.E. Walsh, pp. 303–314. Pittsburgh, Pennsylvania: Creation Science Fellowship.

Horstemeyer, M.F., J.R. Baumgardner, and P.M. Gullett. 2003. What Initiated the Flood cataclysm? In *Proceedings of the Fifth International Conference on Creationism*, ed. R.L. Ivey, pp. 609–621. Pittsburgh, Pennsylvania: Creation Science Fellowship.

Karato, S. 2012. *Deformation of Earth Materials*. Cambridge University Press.

Karato, S., M. Toriumi, and T. Fujii. 1980. Dynamic recrystallization of olivine single crystals during high-temperature creep. *Geophysical Research Letters* 7:649–652.

Kirby, S.H. 1983. Rheology of the lithosphere. *Reviews of Geophysics* 21, no. 6:1458–1487.

Li, L., D. Weidner, P. Raterron, J. Chen, M. Vaughan, S. Mei, and B. Durham. 2006. Deformation of olivine at mantle pressure using the D-DIA. *European Journal of Mineralogy* 18:7–19.

Mainprice, D., G. Barruol, and W.B. IsmaïL. 2000. The Seismic anisotropy of the earth's mantle: from single crystal to polycrystal. In *Earth's Deep Interior: Mineral Physics and Tomography From the Atomic to the*

Global Scale, eds. S.-I. Karato, A. Forte, R. Liebermann, Guysters, and L. Stixrude, pp. 237–264. American Geophysical Union.

Montagner, J.-P., and B.L.N. Kennett. 1996. How to reconcile body-wave and normal-mode reference earth models. *Geophysical Journal International* 125, no. 1:229–248.

Nishihara, Y., D. Tinker, T. Kawazoe, Y. Xu, Z. Jing, K.N. Matsukage, and S. Karato. 2008. Plastic deformation of wadsleyite and olivine at high-pressure and high-temperature using a rotational Drickamer apparatus (RDA). *Physics of the Earth and Planetary Interiors* [*Frontiers and Grand Challenges in Mineral Physics of the Deep Mantle*] 170:156–169.

Ohuchi, T., T. Kawazoe, Y. Higo, K. Funakoshi, A. Suzuki, T. Kikegawa, and T. Irifune. 2015. Dislocation-accommodated grain boundary sliding as the major deformation mechanism of olivine in the earth's upper mantle. *Science Advances* 1, e1500360.

Ohuchi, T., and M. Nakamura. 2007. Grain growth in the forsterite–diopside system. *Physics of the Earth and Planetary Interiors* 160:1–21.

Paladino, A. E., and E. A. Maguire. 1970. Microstructure Development in Yttrium Iron Garnet. *Journal of the American Ceramic Society* 53(2), 98–102. https://doi.org/10.1111/j.1151-2916.1970.tb12019.x

Ringwood, A.E. 1991. Phase transformations and their bearing on the constitution and dynamics of the mantle. *Geochimica et Cosmochimica Acta* 55:2083–2110.

Sherburn, J.A., J.R. Baumgardner, and M.F. Horstemeyer. 2013. New material model reveals inherent tendency in mantle minerals for runaway mantle dynamics. In P*roceedings of the Seventh International Conference on Creationism*, ed. M.F. Horstemeyer. Pittsburgh, Pennsylvania: Creation Science Fellowship.

Sherburn, J.A., M.F. Horstemeyer, D.J. Bammann, and J.R. Baumgardner. 2011. Application of the Bammann inelasticity internal state variable constitutive model to geological materials. *Geophysical Journal International* 184:1023–1036.

Stixrude, L., and C. Lithgow-Bertelloni. 2011. Thermodynamics of mantle minerals - II. Phase equilibria. *Geophysical Journal International* 184:1180–1213.

Tasaka, M., and T. Hiraga. 2013. Influence of mineral fraction on the rheological properties of forsterite + enstatite during grain-size-sensitive creep: 1. Grain size and grain growth laws. *Journal of Geophysical Research: Solid Earth* 118:3970–3990.

Tsujino, N., and Y. Nishihara. 2009. Grain-growth kinetics of ferropericlase at high-pressure. *Physics of the Earth and Planetary Interiors* 174, no. 1–4: 145–152. https://doi.org/10.1016/j.pepi.2008.04.002

Tsujino, N., and Y. Nishihara. 2010. Effect of pressure on grain-growth kinetics of ferropericlase to lower mantle conditions. *Geophysical Research Letters* 37(14), L14304. https://doi.org/10.1029/2010GL043491.

Van der Wal, D., P. Chopra, M. Drury, and J.F. Gerald. 1993. Relationships between dynamically recrystallized grain size and deformation conditions in experimentally deformed olivine rocks. *Geophysical Research Letters* 20:1479–1482.

Wang, Z.-C., S. Mei, S. Karato, and R. Wirth. 1999. Grain growth in CaTiO3-perovskite + FeO-wüstite aggregates. *Physics and Chemistry of Minerals* 27, no. 1:11–19. https://doi.org/10.1007/s002690050235

Yamazaki, D., T. Kato, E. Ohtani, and M. Toriumi. 1996. Grain Growth Rates of MgSiO3 Perovskite and Periclase Under Lower Mantle Conditions. *Science* 274(5295), 2052–2054. https://doi.org/10.1126/science.274.5295.2052

Yamazaki, D., T. Matsuzaki, and T. Yoshino. 2010. Grain growth kinetics of majorite and stishovite in MORB. *Physics of the Earth and Planetary Interiors* [special issue on deep slab and mantle dynamics] 183:183–189.

Zhang, S., S. Karato, J. Fitz Gerald, U.H. Faul, and Y. Zhou. 2000. Simple shear deformation of olivine aggregates. *Tectonophysics* 316:133–152.

THE AUTHORS

Noah Cho is currently a Ph.D. student in computational engineering at Mississippi State University, with an emphasis on computational geophysics. His dissertation research involves development of improved numerical models for the deformation behavior of mantle, combined with an exploration of how that deformation behavior influences the earth mantle's dynamics. The goal of his work is to model the plate tectonics and mantle convection during the Genesis Flood in a more realistic manner than ever before and to gain deeper insight into the physical processes that occurred during this cataclysm.

John Baumgardner has a Ph.D. in geophysics and space physics from UCLA and worked at Los Alamos National Laboratory in computational physics research during most of his scientific career. Since the early 1980's he has undertaken most of the primary research undergirding the concept of catastrophic plate tectonics in connection with Noah's Flood. Beginning in 1997 he served on the Radioisotopes and the Age of the Earth (RATE) team that documented multiple independent lines of radioisotope evidence that the earth is thousands, not billions, of years old. Since 2005 he has been part of a small team that has developed Mendel's Accountant, a computer model for exploring key topics population genetics relating to the origin and history of life. John currently is a senior research associate with Logos Research Associates based in Santa Ana, California, and teaches science apologetics courses at Southern California Seminary in the San Diego area.

Jesse Sherburn has a Ph.D. in mechanical engineering from Mississippi State University and is currently a research mechanical engineer at the U.S. Army Engineer Research and Development Center. He has published over 30 journal articles, technical reports, and conference proceedings in the area of modeling weapon effects on defensive structures relevant to the Department of Defense. His dissertation topic was implementing an internal state variable model into the 2D version of TERRA. The work was used to investigate olivine weakening mechanism in a 2013 ICC paper. He is also an adjunct online professor at Maranatha Baptist University where he frequently teaches a course covering recent creationary research.

Mark Horstemeyer is a professor in the Mechanical Engineering Department at Mississippi State University (MSU) where he holds a Chair position for the Center for Advanced Vehicular Systems in Computational Solid Mechanics. He is also the chief technical officer over the manufacturing and design aspects of CAVS. He has published over 500 journal articles, conference papers, books, and technical reports with a citation H-factor of 52. He has won many awards including the R&D 100 Award, AFS Best Paper Award, Sandia Award for Excellence, the SAE Teetor Award and was a consultant for the Columbia Accident Investigation Board.